

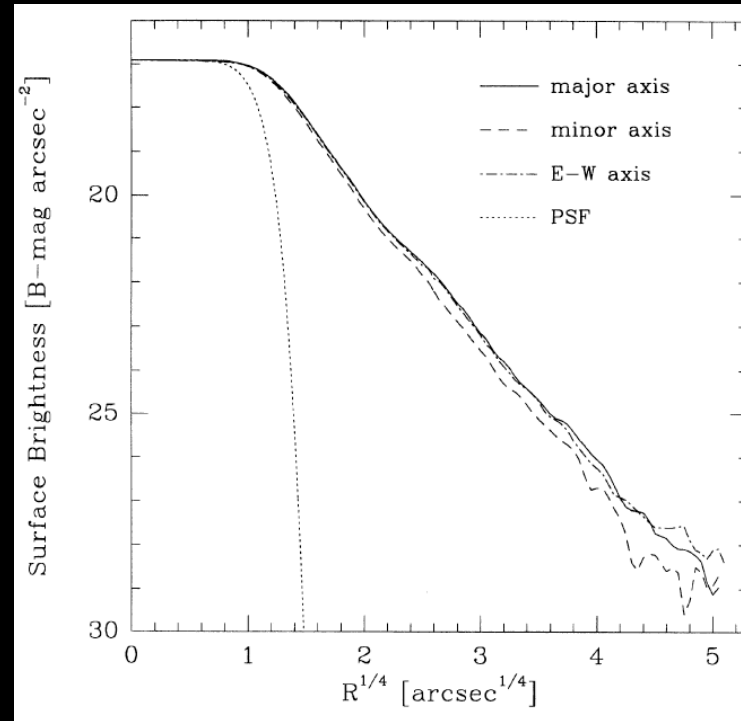
# Galaxies in Equilibrium: Spheroidal Systems

# Review: Surface photometry of spheroids

# “de Vaucouleur profile”

Classic form for massive ellipticals

$$\Sigma(r) = \Sigma_e e^{-7.67(r/r_e)^{1/4} - 1}$$



$r_e$ =“effective radius”, the radius that contains half the light.

$\Sigma_e$ =“effective surface brightness”, the surface brightness at  $r=r_e$ .

$$\Sigma(r) = [\Sigma_e e^{7.67}] e^{-7.67(r/r_e)^{1/4}} = \Sigma_0 e^{-(r/[r_e / 3461])^{1/4}}$$

# Sersic Profile

Generalization of the de Vaucouleur and exponential profiles:

$$\Sigma(r) = \Sigma_e e^{-\kappa[(r/r_e)^{1/n} - 1]}, \quad (6)$$

where  $r_e$  is the effective radius of the galaxy,  $\Sigma_e$  is the surface brightness at  $r_e$ ,  $n$  is the power-law index, and  $\kappa$  is coupled to  $n$  such that half of the total flux is always within  $r_e$ . For  $n \gtrsim 2$ ,  $\kappa \approx 2n - 0.331$ ; at low  $n$ ,  $\kappa(n)$  flattens out toward 0

Exponential: n=1

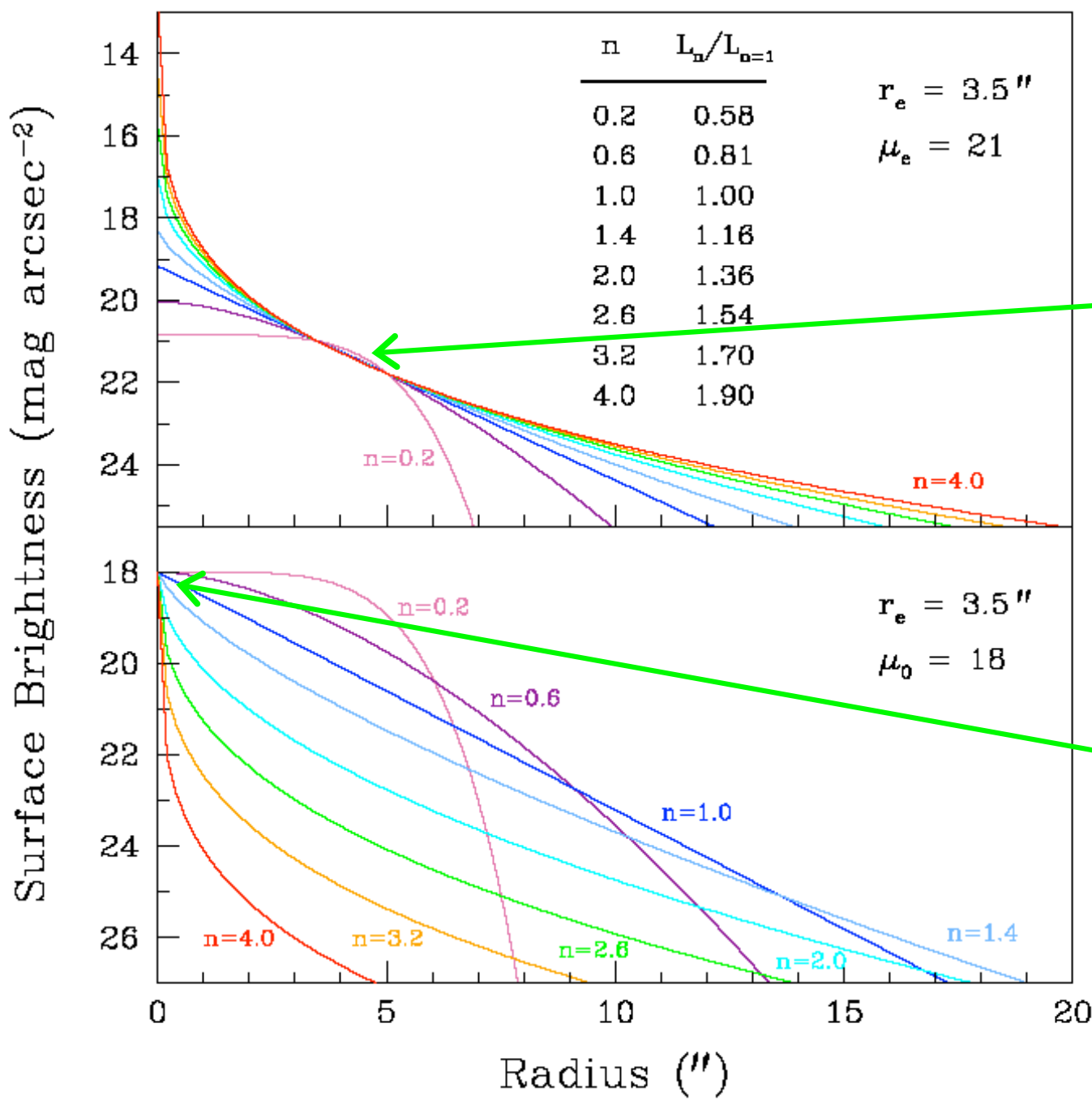
$$\Sigma_e e^{-1.679(r/r_e - 1)}$$

De Vaucouleurs: n=4

$$\Sigma_e e^{-7.67(r/r_e^{1/4} - 1)}$$

# Sersic profiles:

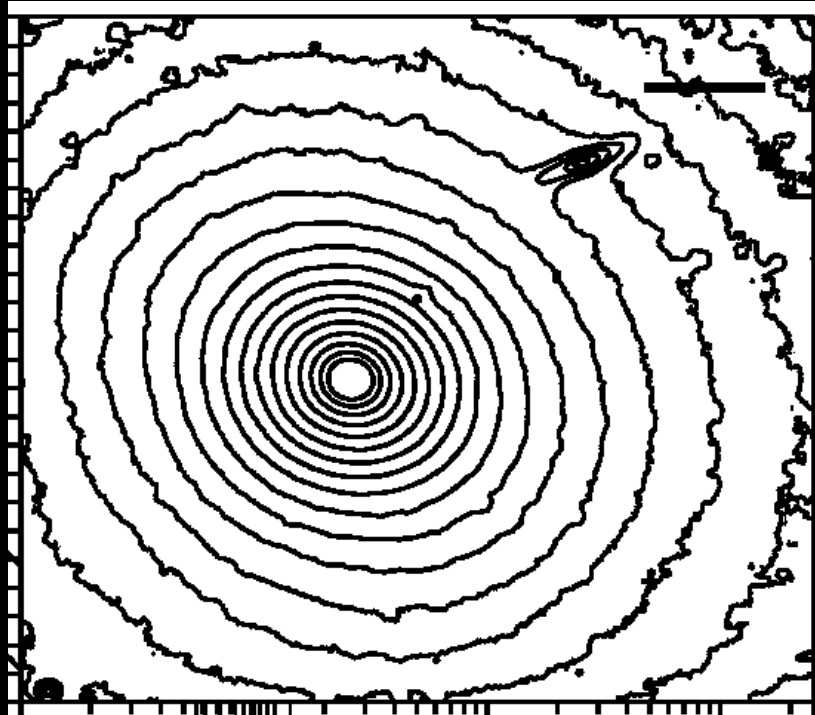
$$\Sigma(r) = \Sigma_e e^{-\kappa[(r/r_e)^{1/n} - 1]}$$



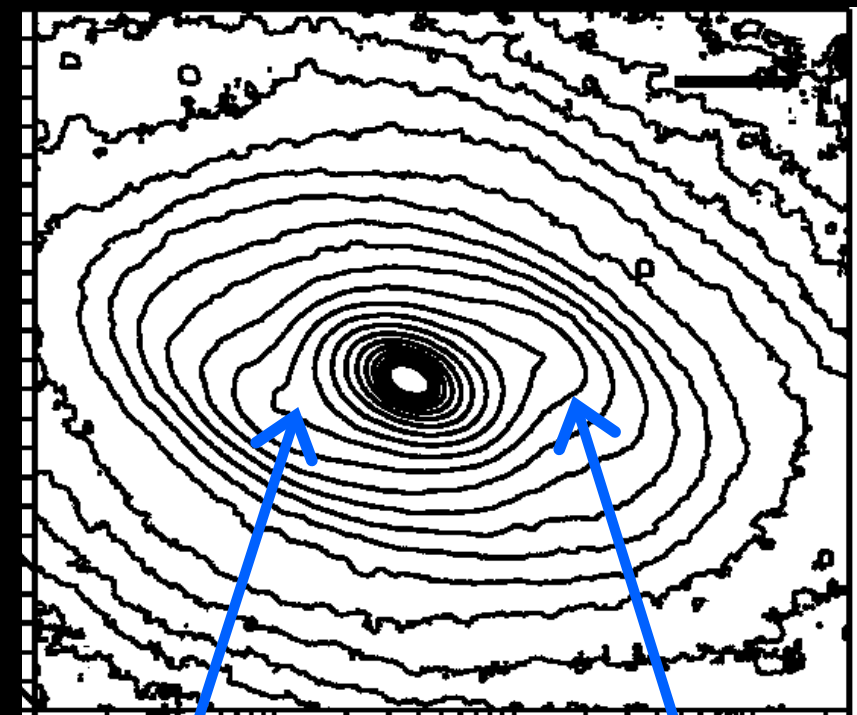
Normalized  
to same  $r_e$ .

Normalized  
to same  $\mu_0$ .

# Often necessary to characterize deviations from ellipticity

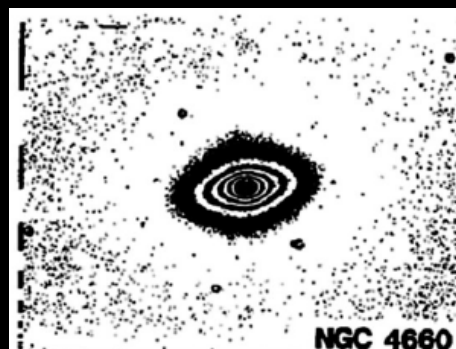


Regular isophotes

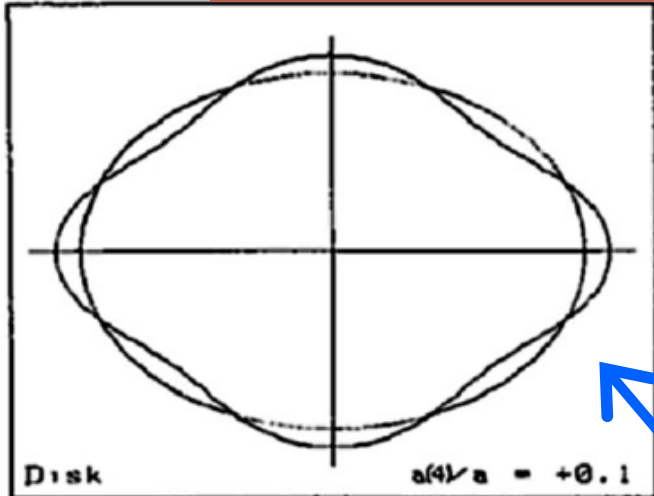


“Disky”

“Boxy”



$$\frac{\delta r(\theta)}{r(\theta)} = \sum_{n=3}^4 [a_n \sin(n\theta) + b_n \cos(n\theta)]$$



Low-order Fourier deviations on the radius as you traverse around the ellipse

$a_4 < 0$  : boxy isophotes  
 $a_4 > 0$  : disky isophotes

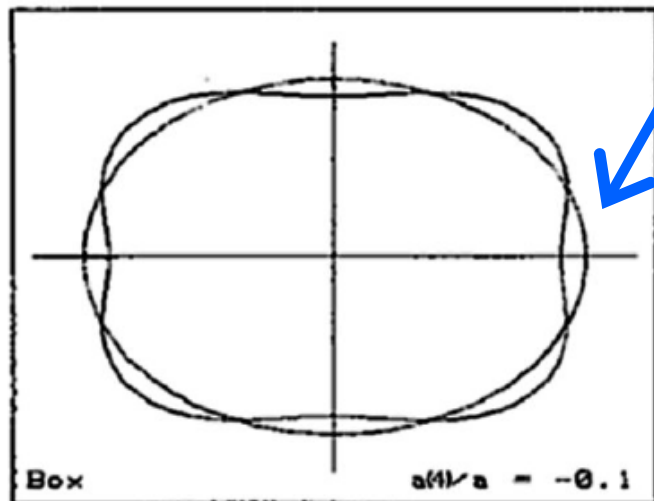
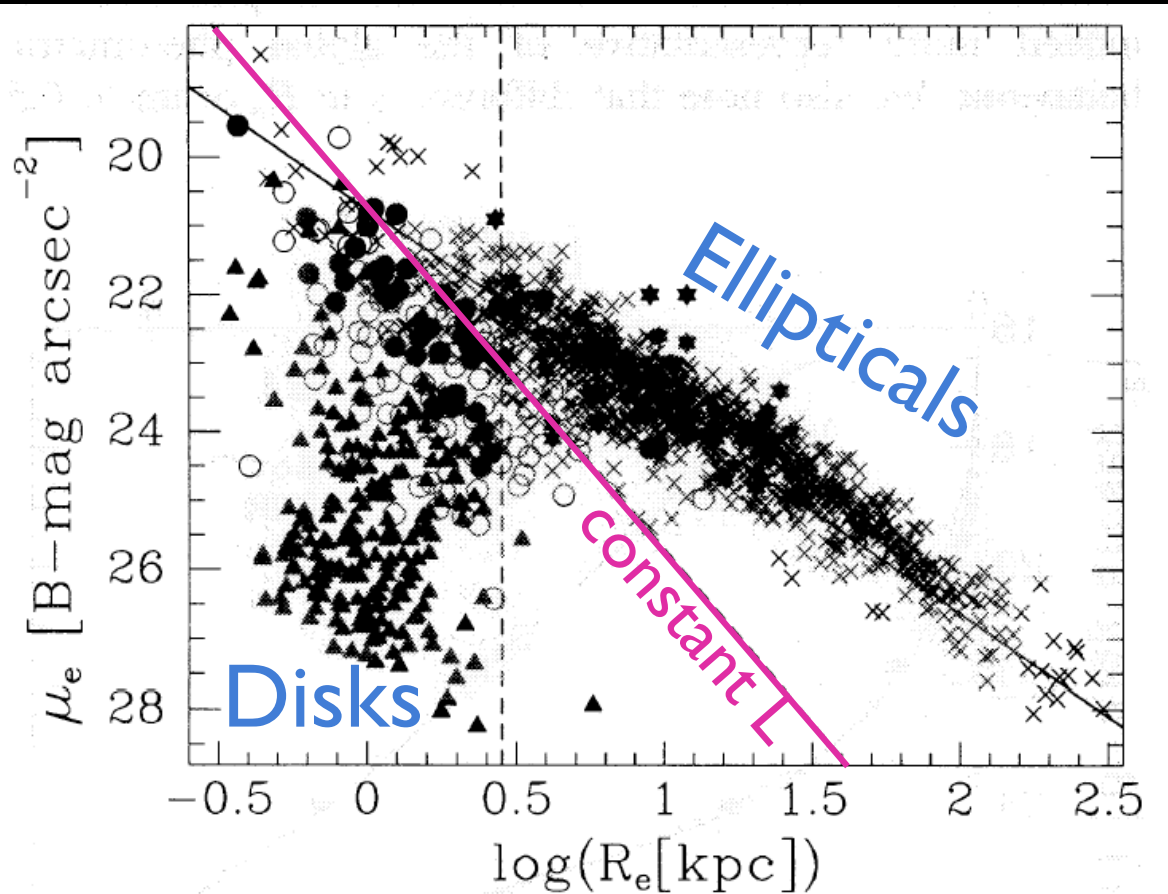


FIGURE 5. — Schematic drawing illustrating isophotes with  $a(4)/a = +0.1$  and  $a(4)/a = -0.1$ .

First:  
How do spirals differ from spheroids?

# Ellipticals and spirals *both* have larger radii with increasing mass

But, ellipticals & spiral disks fall on different sequences in  $\mu_e$  vs  $r_e$ .



**Figure 4.** The  $(\log R_e, \mu_e)$  plane after the addition of literature data. Open circles represent the spiral samples of Kent (1985) and D'Onofrio (1991); filled circles are Es and S0s from CCR and Trevisani (1991); filled triangles are data from Binggeli & Cameron (1992); crosses are data from Schneider et al. (1983), Thomsen & Frandsen (1983), Malumuth & Kirshner (1985), Hoessel & Schneider (1985), Michard (1985), Schombert (1987) and Capaccioli, Piotto & Rampazzo (1988); starred symbols are galaxies hosting a QSO and Seyferts from Malkan (1984) and Malkan et al. (1984). The oblique dashed line is that of constant luminosity,  $M_B = -19.3$ , i.e. the upper limit of the 'ordinary' group; the solid line represents the HK relation.

Capaccioli et al 1992

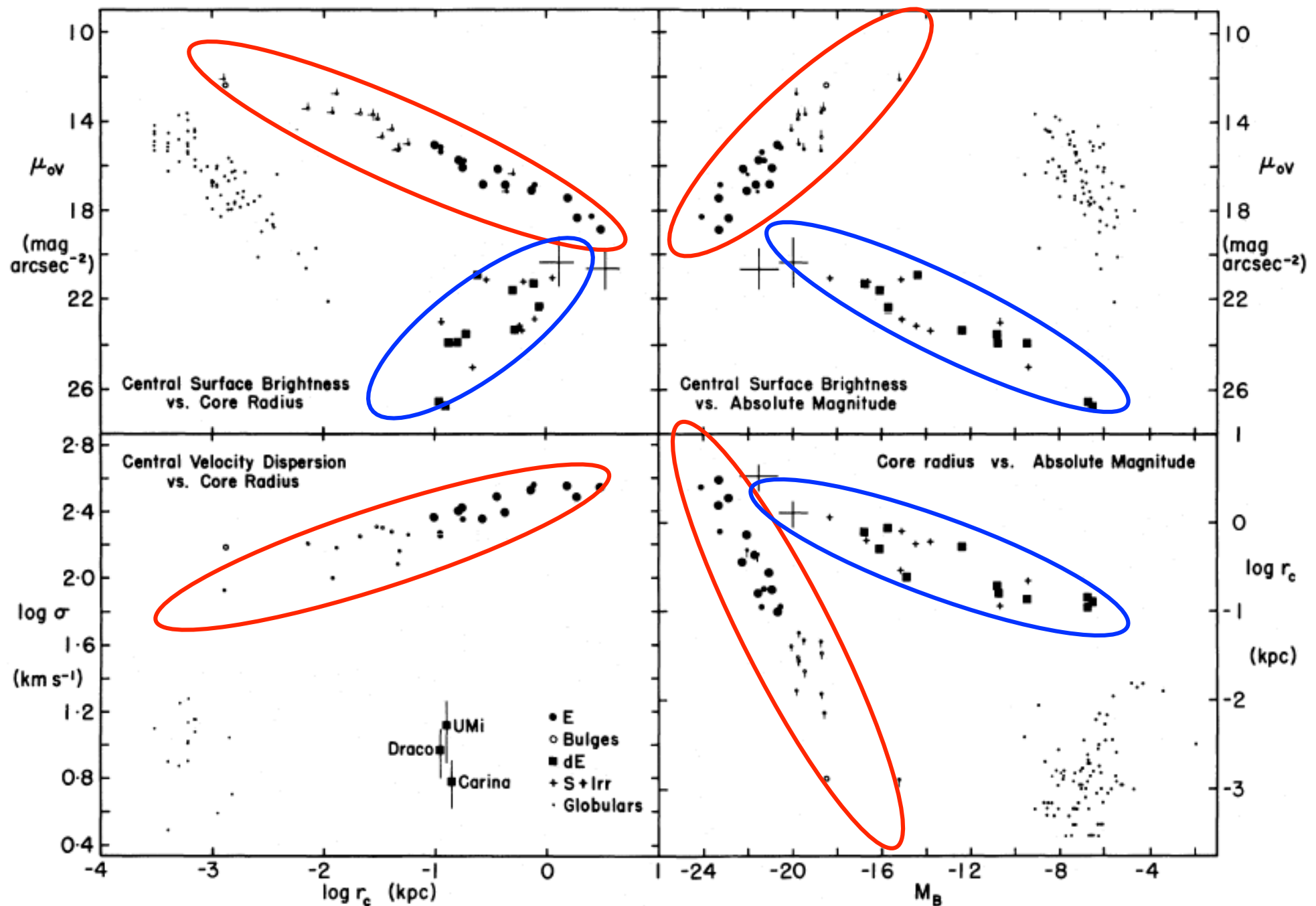


FIG. 3.—Comparison of the core parameter relations for various kinds of stellar systems. Bulges and ellipticals are as in Fig. 2. The dwarf elliptical galaxies are, in order of decreasing luminosity, IC 3349, 12°52, and 13°66 (Virgo Cluster designations from Binggeli, Sandage, and Tarenghi 1984), NGC 147, Fornax, Leo I, Sculptor, Leo II, Draco, Carina, and UMi. Similarly, the dS + Irr galaxies are the generic large disk (two points), LMC, SMC, NGC 6822, WLM, IC 1613, Sextans A, GR 8, and LGS-3. The discrepant globular cluster at upper left ( $\mu_{0V} = 16.38$  mag arcsec $^{-2}$ ,  $\log r_c = -2.42$ ) is, of course,  $\omega$  Cen.

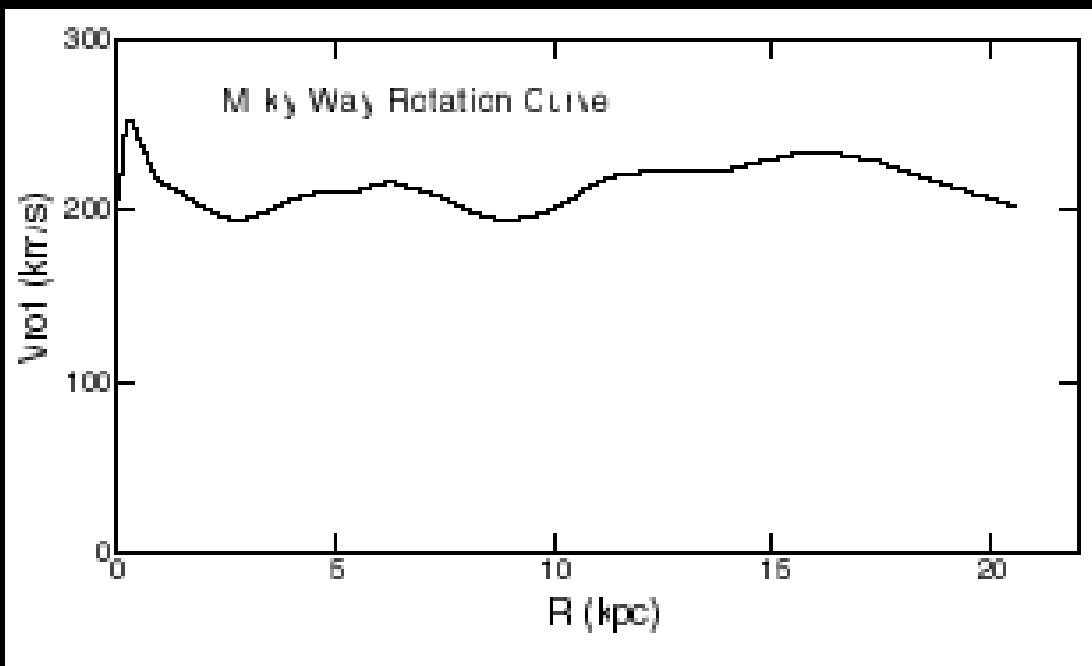
# Different Structure = Different Formation

- Spirals: dissipational gas-rich collapse halted by angular momentum.
- Ellipticals: Disordered formation with random motions being more important than net angular momentum

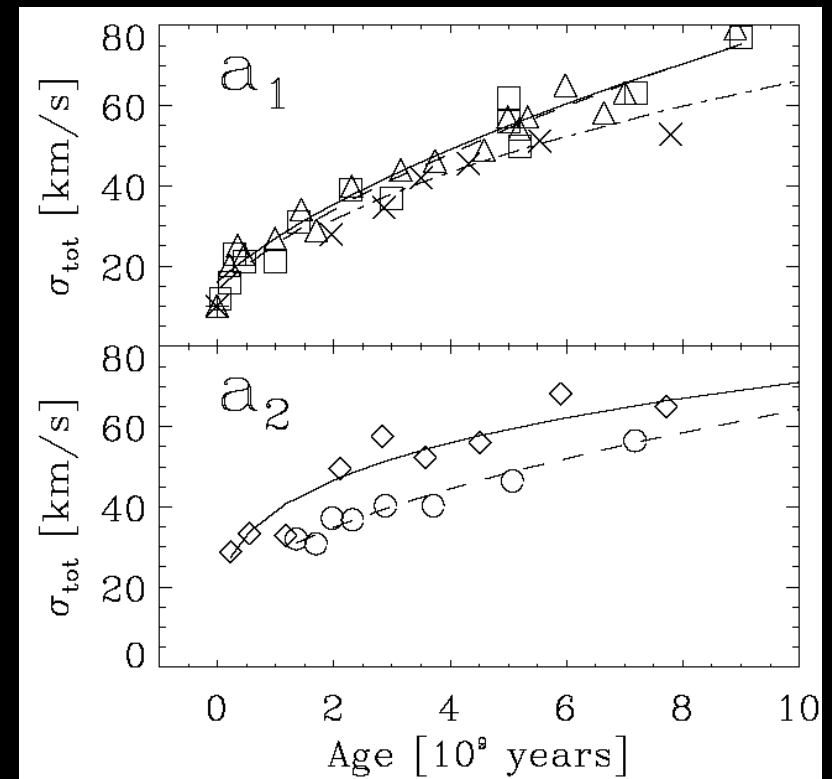
Second:  
The link between kinematics & structure

# Spiral Kinematics:

## Rotation



## Random

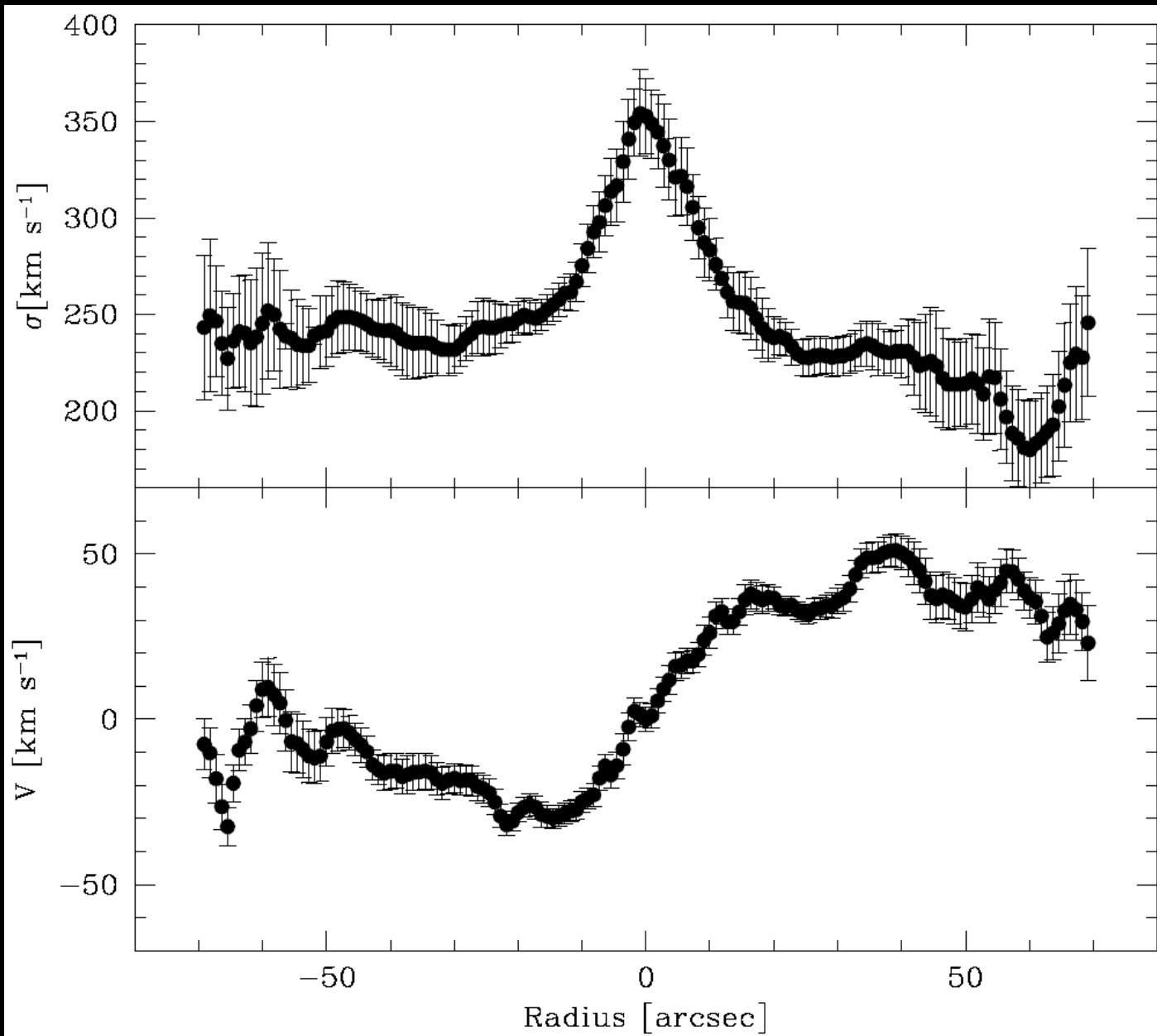


$$V_c/\sigma \sim (200 \text{ km/s})/(50 \text{ km/s}) \sim 4$$

High angular momentum.  
Motion is ordered rather than random.

# Elliptical Kinematics

Supported  
largely by  
random  
motions, not  
ordered  
rotational  
motion

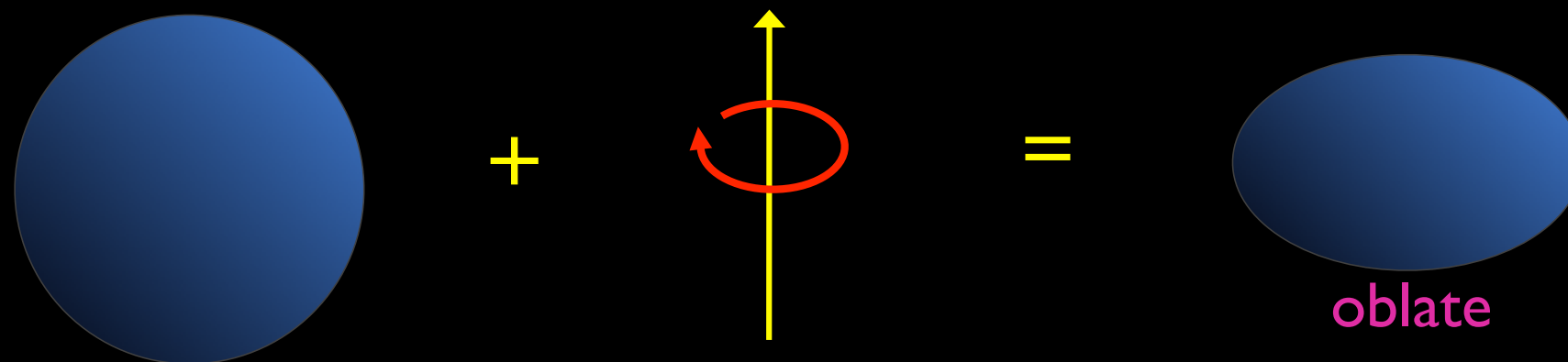


$$V_c / \sigma \sim (50 \text{ km/s}) / (300 \text{ km/s}) \sim 0.17$$

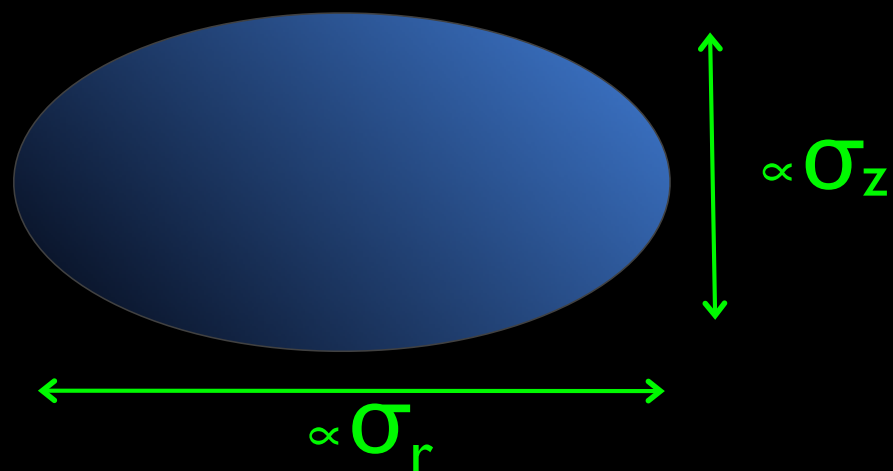
Graham et al 1998

# Two ways kinematics shapes an ellipsoid:

## I. Rotation



## 2. Velocity anisotropy ( $\sigma_r \neq \sigma_\theta \neq \sigma_z$ )



$$(1 - \delta) = \frac{\sigma_z^2}{\sigma_0^2}$$

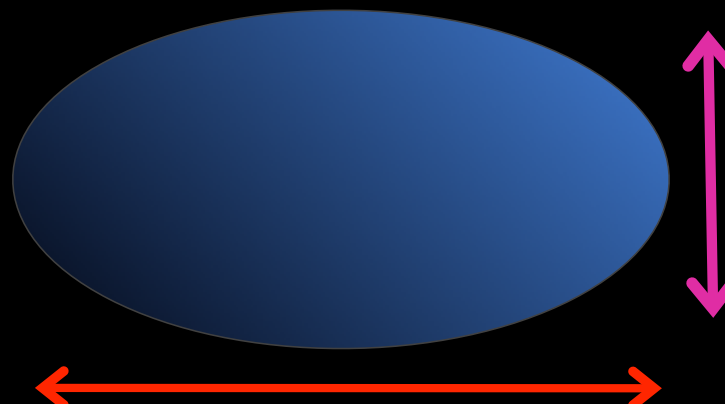
“anisotropy parameter”  $\delta$

# Tensor virial theorem connects kinematics to structure

$$\frac{1}{2} \frac{d^2 I_{jk}}{dt^2} = 2T_{jk} + \Pi_{jk} + W_{jk}$$

	Ordered KE (contains $v_c$ )	Random KE (contains $\sigma$ )	Gravitational PE (contains mass & $b/a$ )
Horizontal equilibrium	$2T_{xx} + \Pi_{xx} + W_{xx} = 0$		

Vertical equilibrium	$2T_{zz} + \Pi_{zz} + W_{zz} = 0$
----------------------	-----------------------------------



TVT: Chandrasekhar 1968

See Binney & Tremaine Ch 4

16 Good lecture notes here: [https://www.ast.cam.ac.uk/~vasily/Lectures/SDSG/sdsg\\_5\\_coll.pdf](https://www.ast.cam.ac.uk/~vasily/Lectures/SDSG/sdsg_5_coll.pdf)

# Tensor virial theorem connects kinematics to structure

If the galaxy is flattened by rotation...

Horizontal equilibrium

$$\text{Ordered KE} \quad \text{Random KE} \quad \text{Gravitational PE}$$
$$2T_{xx} + \Pi_{xx} + W_{xx} = 0$$

Vertical equilibrium

$$2T_{zz} + \Pi_{zz} + W_{zz} = 0$$

This term is zero, since all the rotation is around the z axis

These terms are equal, if isotropic velocity dispersions

The ratio of these depends only on the geometry of the galaxy (i.e. the axial ratio b/a)

# Tensor virial theorem connects kinematics to structure

If the galaxy is flattened by velocity anisotropy ( $\sigma_r \neq \sigma_\theta \neq \sigma_z$ )...

Horizontal equilibrium

$$\text{Ordered KE} + \text{Random KE} + \text{Gravitational PE} = 0$$
$$2T_{xx} + \Pi_{xx} + W_{xx} = 0$$

Vertical equilibrium

$$2T_{zz} + \Pi_{zz} + W_{zz} = 0$$

These terms are zero, since there's no bulk flow in equilibrium

The ratio of these terms depends only on  $\sigma_z/\sigma_x$

The ratio of these depends only on the geometry of the galaxy (i.e. the axial ratio  $b/a$ )

	Ordered KE	Random KE	Gravitational PE
Horizontal equilibrium	$2T_{xx} + \Pi_{xx} + W_{xx} = 0$		

Vertical equilibrium	$2T_{zz} + \Pi_{zz} + W_{zz} = 0$
----------------------	-----------------------------------

Taking a ratio & making approximations yields connection between observed velocity and predicted axial ratio  $a/b$

$v_m$  is a mean rotation speed, and  $\sigma$  is an averaged velocity dispersion; see Davies et al 1983

$$\frac{v_m}{\bar{\sigma}} \simeq \sqrt{\frac{1 - b/a}{b/a}}$$

Flattened by rotation

E3 needs:  $\frac{v_m}{\bar{\sigma}} \sim 0.8$

A ton of rotation

$$\frac{\sigma_z}{\sigma_0} \simeq \left(\frac{b}{a}\right)^{0.45}$$

Flattened by anisotropy

E3 needs:  $\frac{\sigma_z}{\sigma_0} \sim 0.9$

A little anisotropy

*Begin math detour giving fuller derivation  
of flattening calculation...*

Test if the observed rotation is enough to provide the necessary flattening

Assume the galaxy is in equilibrium and obeys the tensor virial theorem:

$$\frac{1}{2} \frac{d^2 I_{jk}}{dt^2} = 2T_{jk} + \Pi_{jk} + W_{jk}$$

(a system of 9 equations which dynamical systems must obey, derived by taking the 3 momentum equations of the Jeans equation, multiplying by each of the 3 space coordinates, and integrating over all space)

# The tensor virial theorem

$$\frac{1}{2} \frac{d^2 I_{jk}}{dt^2} = 2T_{jk} + \Pi_{jk} + W_{jk}$$

$$T_{jk} = \frac{1}{2} \int \rho \overline{v_j v_k} d^3 \vec{x}$$

Kinetic energy from bulk flow

$$\Pi_{jk} = \int \rho \sigma_{jk}^2 d^3 \vec{x}$$

Kinetic energy from random motion (x2)

$$\sigma_{jk}^2 = (v_j - \overline{v_j})(v_k - \overline{v_k})$$

# The tensor virial theorem

$$\frac{1}{2} \frac{d^2 I_{jk}}{dt^2} = 2T_{jk} + \Pi_{jk} + W_{jk}$$

$$W_{jk} = \int \rho x_k \frac{\partial \phi}{\partial x_j} d^3 \vec{x}$$

Gravitational potential energy tensor

$$I_{jk} = \int \rho x_j x_k d^3 \vec{x}$$

Moment of inertia tensor

All these terms are symmetric:

$$T_{jk} = T_{kj}$$

$$\Pi_{jk} = \Pi_{kj}$$

$$W_{jk} = W_{kj}$$

$$I_{jk} = I_{kj}$$

# The tensor virial theorem:

Assume steady state:

$$\cancel{\frac{1}{2} \frac{d^2 I_{jk}}{dt^2}} = 2T_{jk} + \Pi_{jk} + W_{jk}$$

# The tensor virial theorem:

$$\frac{1}{2} \frac{d^2 I_{jk}}{dt^2} = 2T_{jk} + \Pi_{jk} + W_{jk}$$

The trace of the tensor reproduces the more familiar (but less useful) scalar virial theorem

$$2K + W = 0$$

$$K = \text{Trace}(T_{jk} + \frac{1}{2}\Pi_{jk})$$

Kinetic Energy

$$W = \text{Trace}(W_{jk})$$

Gravitational Potential Energy

In steady state....

The tensor virial theorem:

$$\frac{1}{2} \frac{d^2 I_{jk}}{dt^2} = 2T_{jk} + \Pi_{jk} + W_{jk}$$

This set of equations can be reduced to three if one rotates the coordinate system to be along the principal axes:

$$W_{jk} = T_{jk} = \Pi_{jk} = 0 \quad j \neq k$$

We can further reduce these by considering an oblate, axisymmetric system:

$$W_{xx} = W_{yy}$$

$$T_{xx} = T_{yy}$$

$$\Pi_{xx} = \Pi_{yy}$$

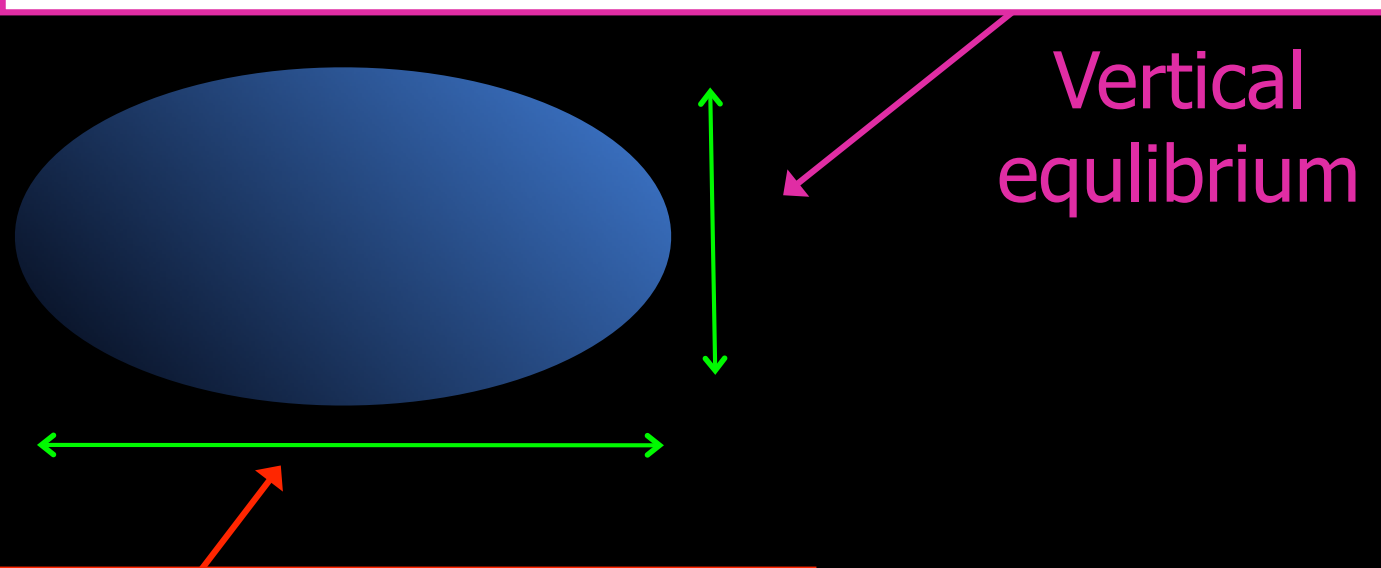
# The tensor virial theorem:

$$\frac{1}{2} \frac{d^2 I_{jk}}{dt^2} = 2T_{jk} + \Pi_{jk} + W_{jk}$$

This leaves us with only two equations for an oblate, axisymmetric galaxy in equilibrium:

$$2T_{zz} + \Pi_{zz} + W_{zz} = 0$$

Horizontal equilibrium



Vertical equilibrium

$$2T_{xx} + \Pi_{xx} + W_{xx} = 0$$

# If the galaxy is flattened by rotation

This term is zero,  
since all the rotation  
is around the z axis

$$2T_{xx} + \Pi_{xx} + W_{xx} = 0$$

Horizontal  
equilibrium

$$2T_{zz} + \Pi_{zz} + W_{zz} = 0$$

Vertical  
equilibrium

These terms  
are equal, if  
isotropic  
velocity  
dispersions

The ratio of these  
depends only on  
the geometry of the  
galaxy (i.e. the  
axial ratio b/a)

# If the galaxy is flattened by rotation

$$\Pi_{xx} = \Pi_{zz}$$

Take the ratio of the eqns:

$$2T_{xx} + \Pi_{xx} + W_{xx} = 0$$

Horizontal  
equilibrium

~~$$2T_{zz} + \Pi_{zz} + W_{zz} = 0$$~~

Vertical  
equilibrium

$$\frac{2T_{xx}}{\Pi_{xx}} + 1 = \frac{W_{xx}}{W_{zz}}$$

# If the galaxy is flattened by velocity anisotropy

The ratio of these depends only on the geometry of the galaxy (i.e. the axial ratio  $b/a$ )

The diagram shows a horizontally flattened galaxy represented by a red rectangle. Inside, there are two horizontal layers: a top layer in a red-bordered box and a bottom layer in a pink-bordered box. The top layer contains the equation  $2T_{xx} + \Pi_{xx} + W_{xx} = 0$ . The bottom layer contains the equation  $2T_{zz} + \Pi_{zz} + W_{zz} = 0$ . Three ovals (yellow, green, and cyan) are drawn around the terms  $2T_{xx}$ ,  $\Pi_{xx}$ , and  $W_{xx}$  respectively in the top equation, and around the terms  $2T_{zz}$ ,  $\Pi_{zz}$ , and  $W_{zz}$  respectively in the bottom equation. Arrows point from the text below to these ovals.

$$2T_{xx} + \Pi_{xx} + W_{xx} = 0$$
$$2T_{zz} + \Pi_{zz} + W_{zz} = 0$$

Horizontal equilibrium

Vertical equilibrium

These terms are zero, since there's no bulk flow

The ratio of these terms depends only on the ratio of the vertical to horizontal velocity dispersions.

# If the galaxy is flattened by velocity anisotropy

$$2T_{xx} + \Pi_{xx} + W_{xx} = 0$$

Horizontal equilibrium

$$2T_{zz} + \Pi_{zz} + W_{zz} = 0$$

Vertical equilibrium

Taking the ratio of the eqn's:

$$\frac{\Pi_{xx}}{\Pi_{zz}} = \frac{W_{xx}}{W_{zz}}$$

We can characterize the velocity anisotropy with a parameter  $\delta$  such that:

$$(1 - \delta) = \frac{\Pi_{zz}}{\Pi_{xx}} = \frac{\sigma_z^2}{\sigma_0^2}$$

$\delta = 0$ : isotropic velocity ( $\sigma_z = \sigma_0$ )

$1 > \delta > 0$ : anisotropic velocity ( $\sigma_z < \sigma_0$ )

And in terms of the anisotropy parameter:

$$\Pi_{zz} = (1 - \delta)\Pi_{xx}$$

Take the ratio  
of the 2 eqns:  
(general case)

$$\frac{2T_{xx} + \Pi_{xx}}{2T_{zz} + \Pi_{zz}} = \frac{W_{xx}}{W_{zz}}$$

In all cases assume:

$$T_{zz} = 0$$

Define a mass-weighted mean rotational velocity  $v_0$  and a mean random velocity  $\sigma_0$ ,  
such that:

$$T_{xx} + T_{yy} = 2T_{xx} = \frac{1}{2}Mv_0^2$$

and  $\Pi_{xx} = M\sigma_0^2$

or  $\Pi_{zz} = (1 - \delta)M\sigma_0^2$

$$2T_{xx} = \frac{1}{2}Mv_0^2$$

$$\Pi_{xx} = M\sigma_0^2$$

$$T_{zz} = 0$$

$$\frac{2T_{xx} + \Pi_{xx}}{2T_{zz} + \Pi_{zz}} = \frac{W_{xx}}{W_{zz}}$$

$$\Pi_{zz} = (1 - \delta)M\sigma_0^2$$

**Substituting:**

$$\frac{\frac{1}{2}Mv_0^2 + \Pi_{xx}}{(1 - \delta)\Pi_{xx}} = \frac{W_{xx}}{W_{zz}}$$

$$\frac{\frac{1}{2}Mv_0^2}{M\sigma_0^2} + 1 = (1 - \delta)\frac{W_{xx}}{W_{zz}}$$

$$\left(\frac{v_0}{\sigma_0}\right)^2 = 2(1 - \delta)\frac{W_{xx}}{W_{zz}} - 2$$

-1 if flattened  
only by rotation  
(i.e. isotropic)

$$\left(\frac{v_0}{\sigma_0}\right)^2 = 2(1 - \delta) \frac{W_{xx}}{W_{zz}} - 2$$

Related to the observable  
rotation speed  $v_m$  and mean  
velocity dispersion within  $r_e/2$

$$\frac{v_m}{\bar{\sigma}} \simeq \frac{\pi}{4} \frac{v_0}{\sigma_0}$$

Related to the  
observed axial  
ratio ( $a/b$ )

$$\frac{W_{xx}}{W_{zz}} \simeq \left(\frac{a}{b}\right)^{0.89}$$

If flattened by rotation:

$$\left(\frac{v_0}{\sigma_0}\right)^2 = 2(1 - \delta) \frac{W_{xx}}{W_{zz}} - 2$$

$$\frac{v_m}{\bar{\sigma}} \simeq \frac{\pi}{4} \frac{v_0}{\sigma_0}$$

$$\frac{W_{xx}}{W_{zz}} \simeq \left(\frac{a}{b}\right)^{0.89}$$

$$\frac{v_0}{\sigma_0} \simeq \frac{4}{\pi} \sqrt{\frac{1 - b/a}{b/a}}$$

After approximating:

$$\sqrt{2} \simeq \frac{4}{\pi}$$

$$0.89 \approx 1$$

Gives a simple relationship between the intrinsic ellipticity and the ratio of rotation speed to velocity dispersion. If a galaxy follows this relation, it's probably flattened by rotation!

If flattened by velocity anisotropy:

$$\left(\frac{v_0}{\sigma_0}\right)^2 = 2(1 - \delta) \frac{W_{xx}}{W_{zz}} - 2$$

$$\frac{W_{xx}}{W_{zz}} \simeq \left(\frac{a}{b}\right)^{0.89}$$

$$\frac{\Pi_{xx}}{\Pi_{zz}} = \frac{W_{xx}}{W_{zz}}$$

$$\rightarrow \frac{\sigma_z}{\sigma_0} = \sqrt{\frac{W_{zz}}{W_{xx}}}$$

$$\frac{\sigma_z}{\sigma_0} \simeq \left(\frac{b}{a}\right)^{0.45}$$

Gives a simple relationship between the intrinsic ellipticity and the anisotropy.

What sort of rotations or anisotropies are needed to make an E3 ( $b/a=0.7$ )?

$$\frac{\sigma_z}{\sigma_0} \simeq \left(\frac{b}{a}\right)^{0.45}$$

Requires:

$$\frac{\sigma_z}{\sigma_0} \sim 0.9$$

$$\frac{v_0}{\sigma_0} \simeq \frac{4}{\pi} \sqrt{\frac{1 - b/a}{b/a}}$$

Requires:

$$\frac{v_m}{\bar{\sigma}} \sim 0.8$$

using  $\frac{v_m}{\bar{\sigma}} \simeq \frac{\pi}{4} \frac{v_0}{\sigma_0}$

Observed  
quantities

So an E3 either has **mild anisotropy**, or **large rotation**

*End of math detour.*

# Real data!

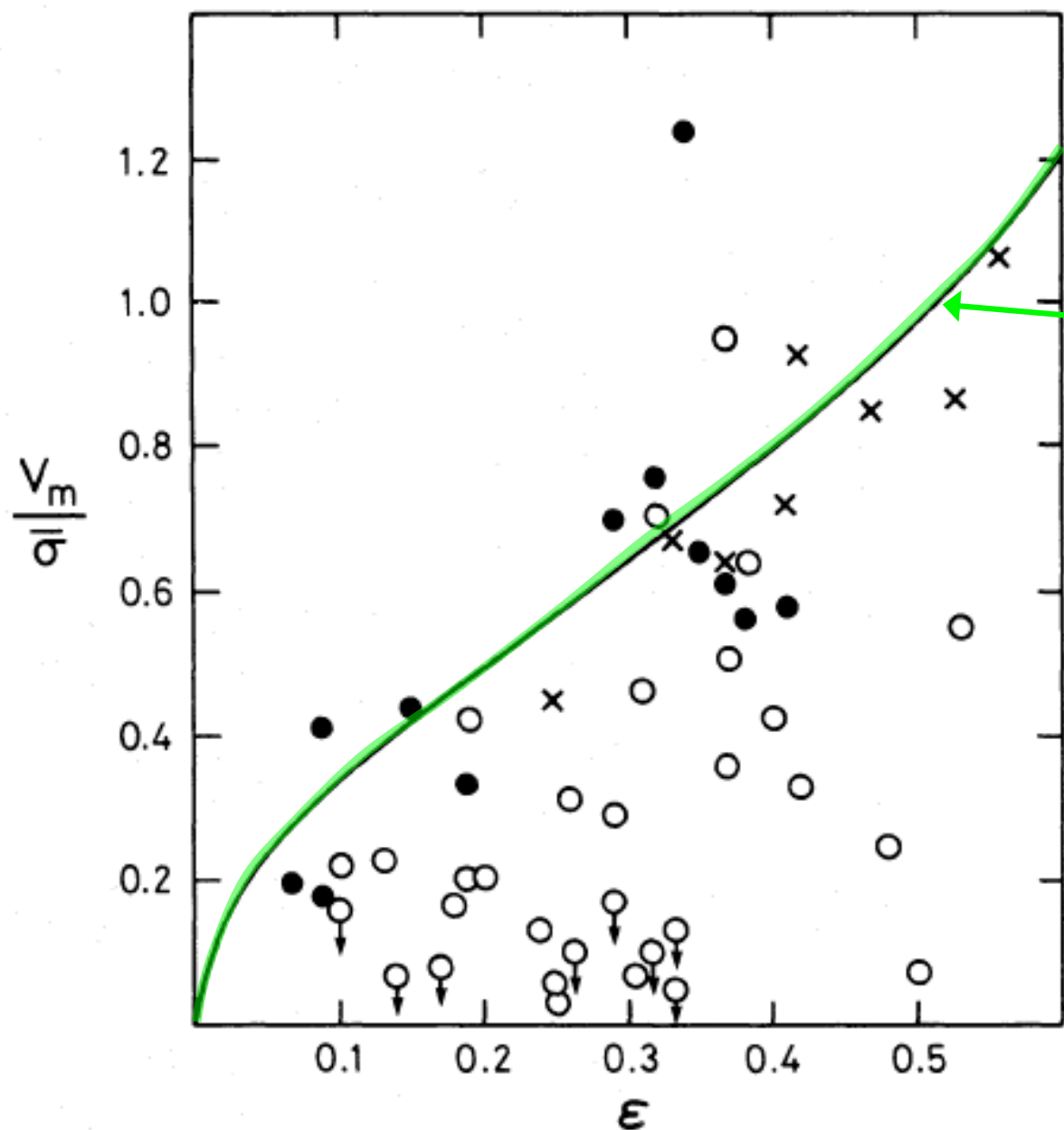


FIG. 3.—The quantity  $V_m/\bar{\sigma}$  against ellipticity. Ellipticals with  $M_B^{UH} > -20.5$  are shown as filled circles; ellipticals with  $M_B^{UH} < -20.5$ , as open circles; and the bulges of disk galaxies, as crosses. The solid line shows the  $(V/\sigma, \epsilon)$ -relation for oblate galaxies with isotropic velocity dispersions (Binney 1978). Davies et al 1983

$$\frac{v_m}{\bar{\sigma}} \simeq \sqrt{\frac{1 - b/a}{b/a}}$$

- Bright ellipticals are flat because their velocity dispersions are not the same in all directions
- Faint ellipticals & bulges (solid pts & x's) are flattened by rotation.

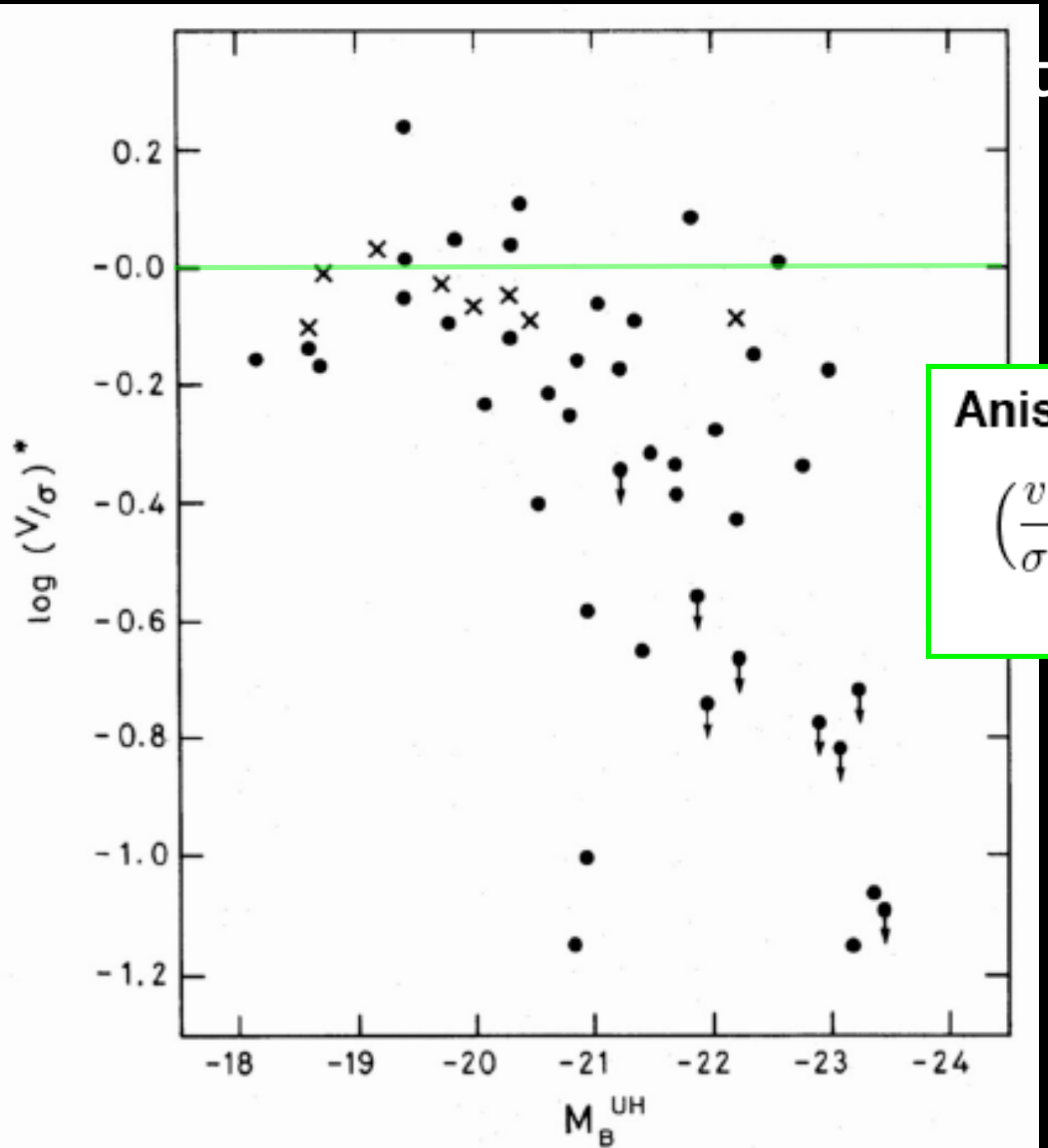


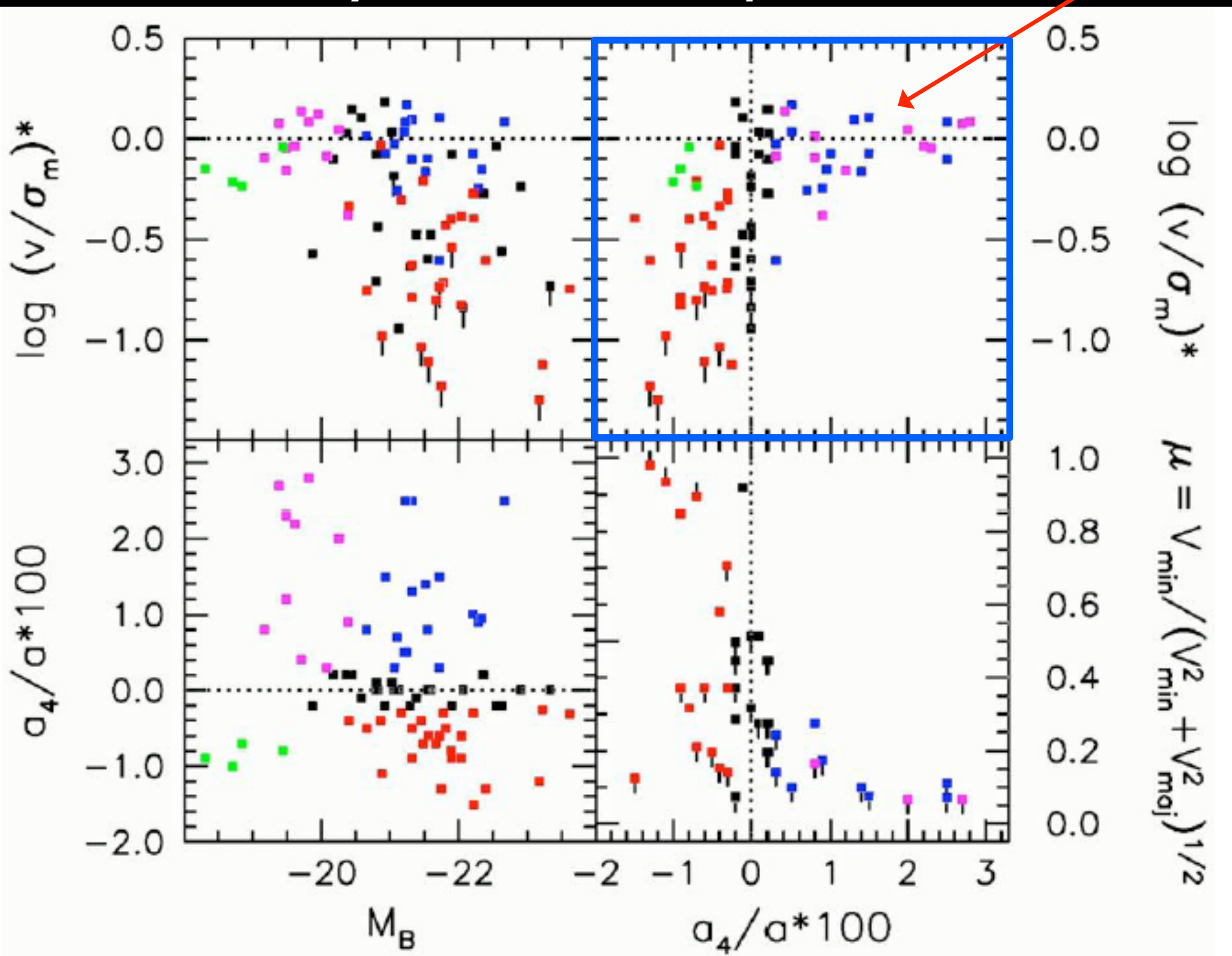
FIG. 4.— $\log(V/\sigma)^*$  against absolute magnitude. Ellipticals are shown as filled circles and the bulges as crosses;  $(V/\sigma)^*$  is defined in § IIIb.

Anisotropy parameter:

$$\left(\frac{v}{\sigma}\right)^* \equiv \frac{v/\sigma}{\sqrt{\frac{1-b/a}{b/a}}} = \frac{(v/\sigma)_{\text{observed}}}{(v/\sigma)_{\text{rot. flattened}}}$$

Davies 1983

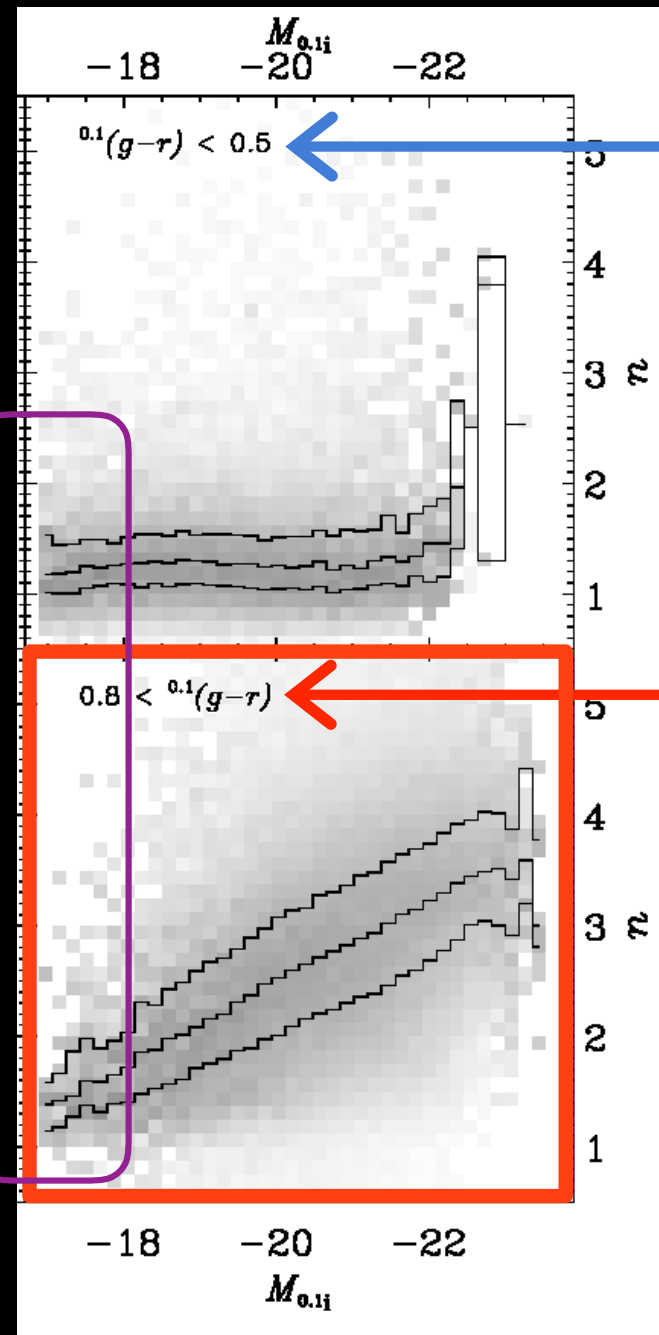
# Rotationally flattened ellipticals are also disky



Second:  
Trends among spheroidal galaxies

# Smaller ellipticals = smaller Sersic $n$

Similar  
structure  
for dwarfs  
( $dE \sim dI_{rr}$ )

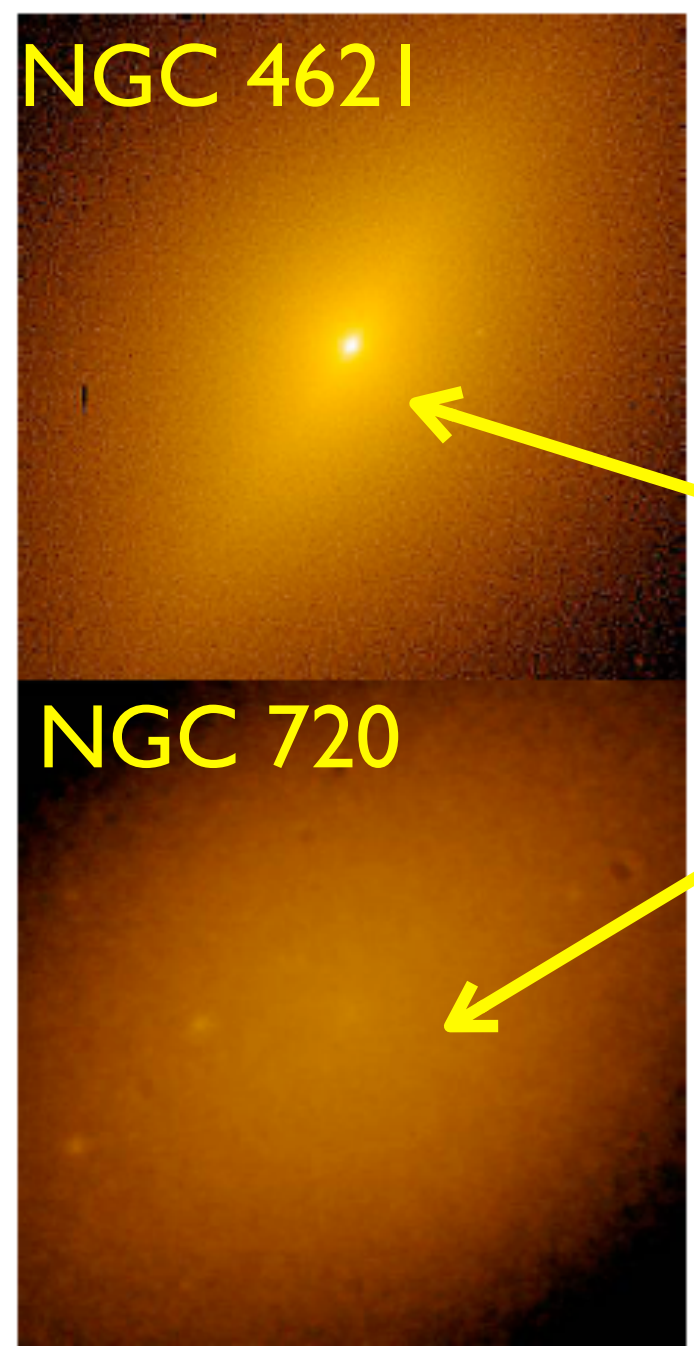


Blue galaxies  
(presumably  
late-type)

Red galaxies  
(presumably  
early-type)

# Low and high mass ellipticals differ in their **very** centers

NGC 4621

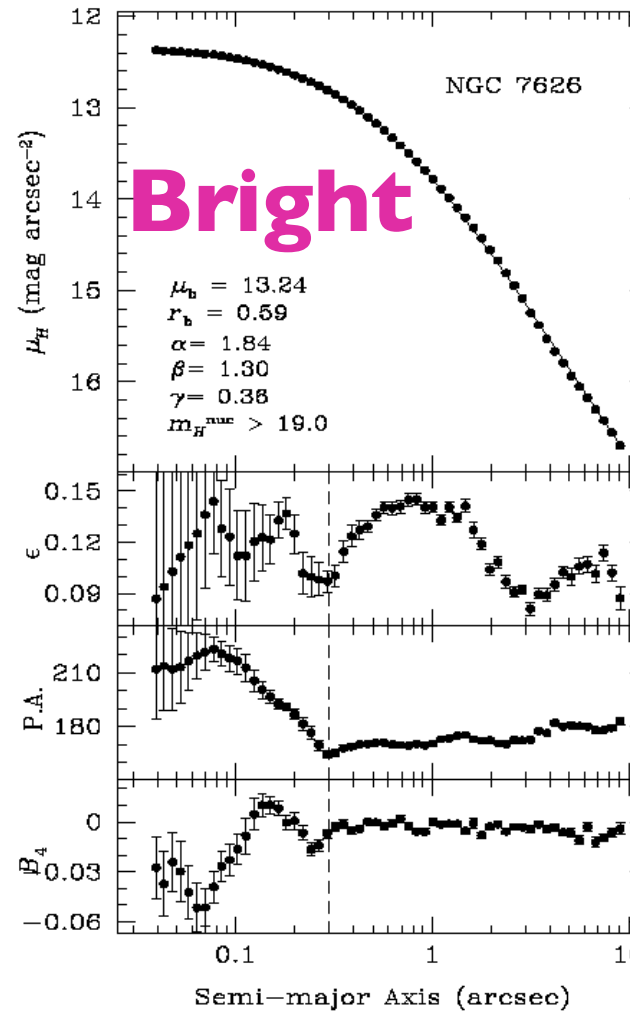
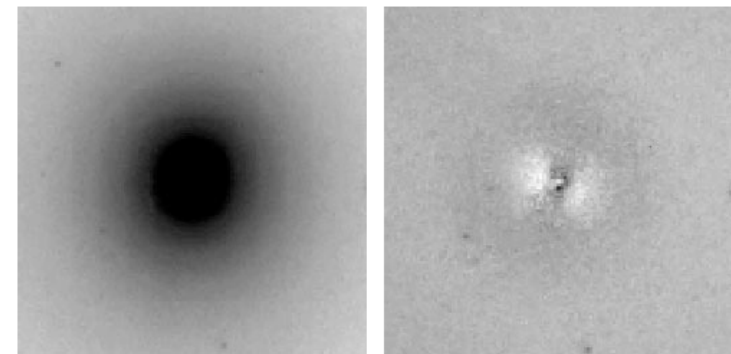
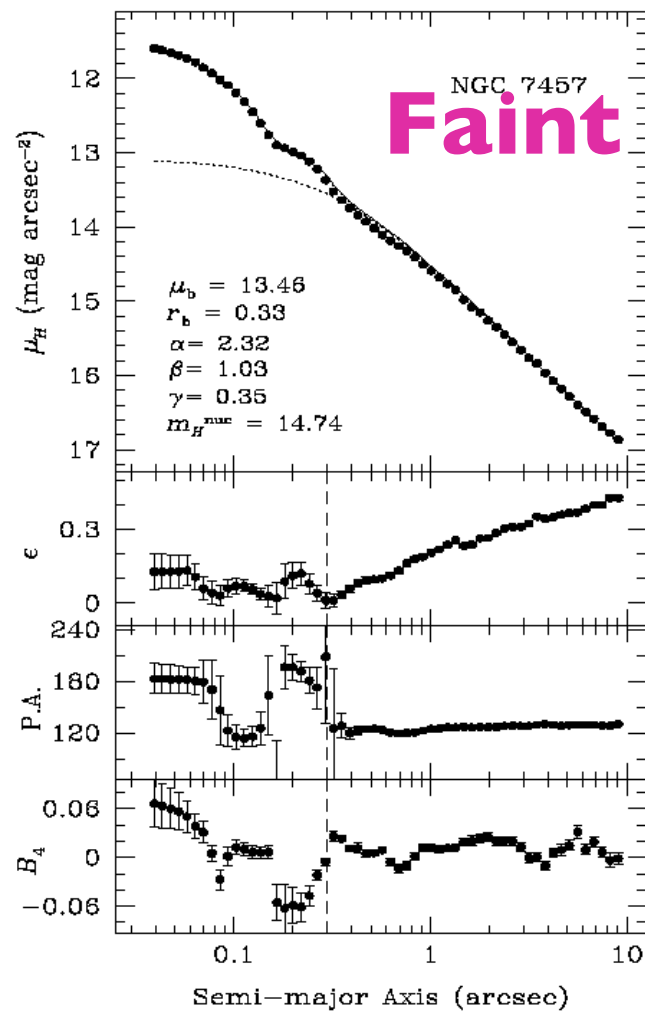
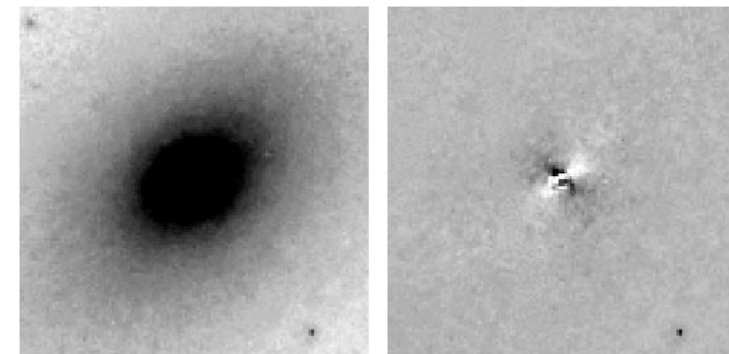


NGC 720

When imaged at HST resolution:

- Faint ellipticals have dense cusps
- Bright ellipticals have flat cores

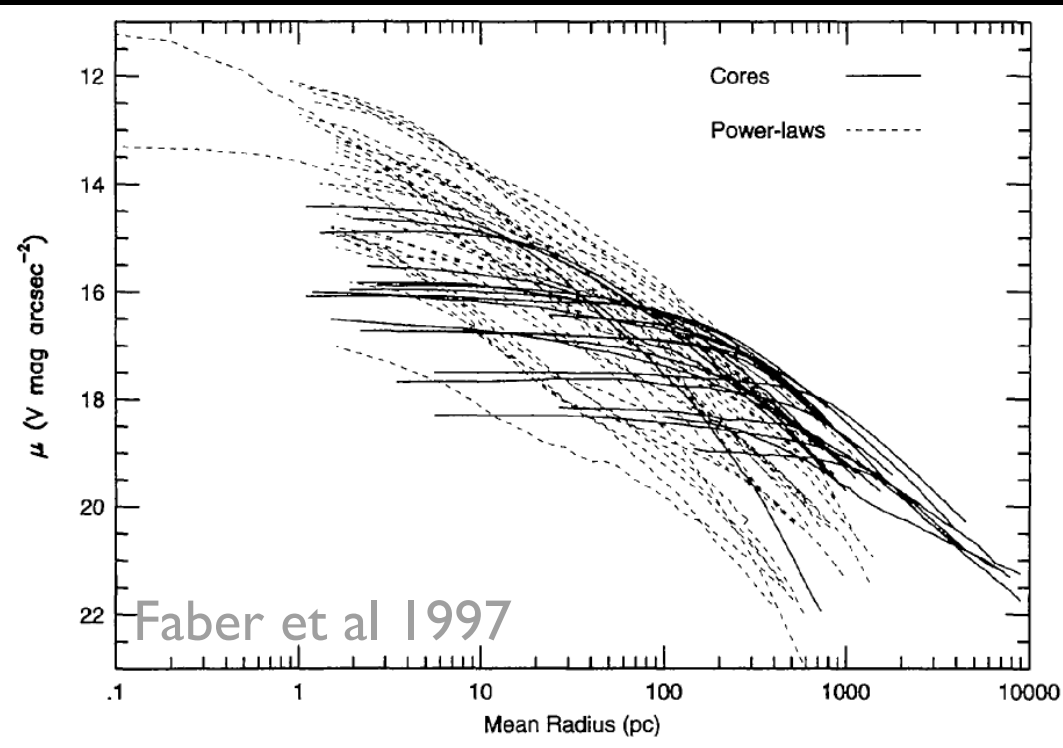
# NICMOS data from HST



These inner profiles are frequently characterized with a “Nuker Law”

$$I(r) = I_b 2^{(\beta - \gamma)/\alpha} \left( \frac{r}{r_b} \right)^{-\gamma} \left[ 1 + \left( \frac{r}{r_b} \right)^\alpha \right]^{(\gamma - \beta)/\alpha},$$

as  $I(r) \propto r^{-\beta}$  at  $r^\alpha \gg r_b^\alpha$ , and  $I(r) \propto r^{-\gamma}$  at  $r^\alpha \ll r_b^\alpha$ .



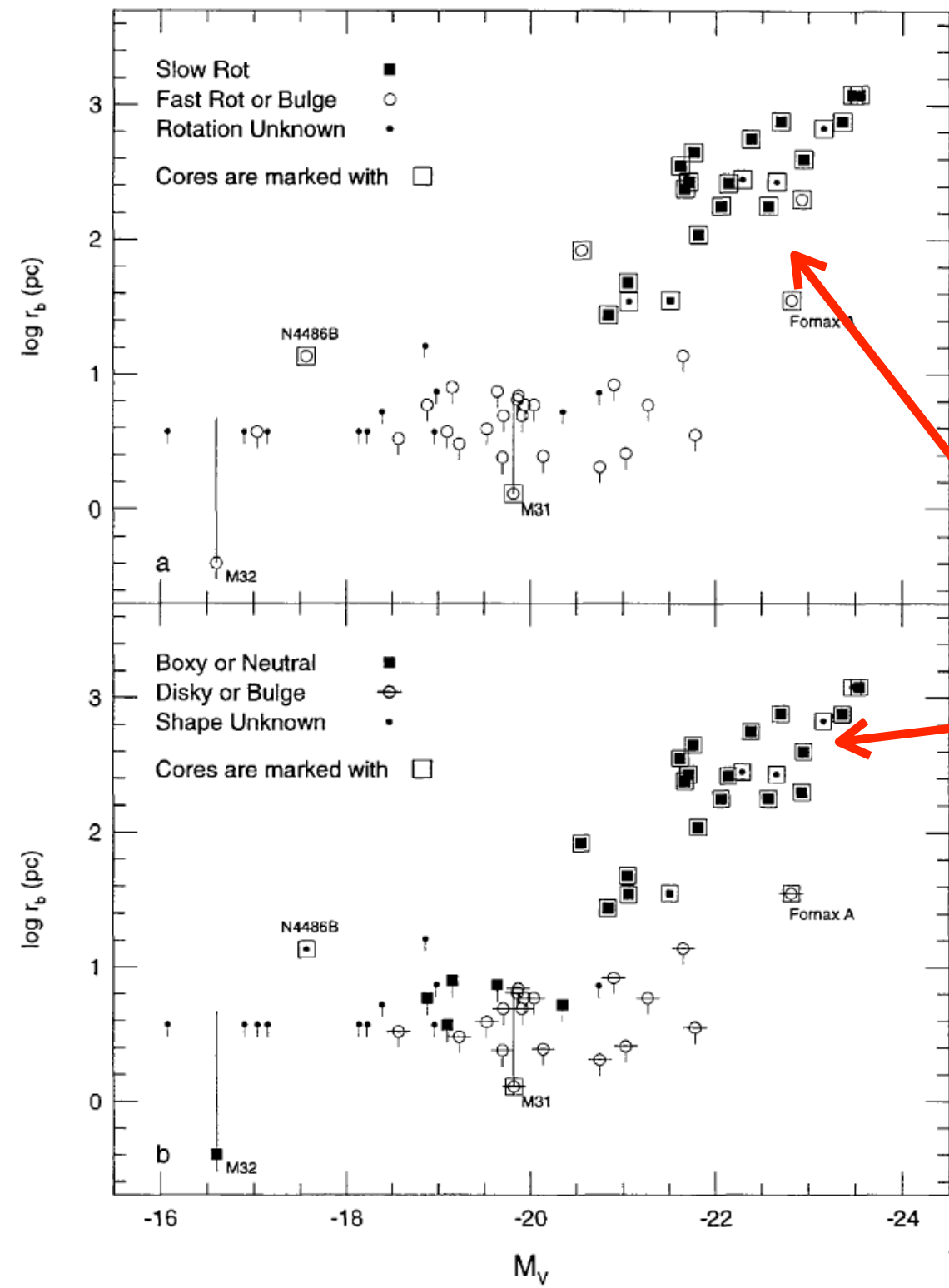
Lauer et al 1995

A double power law defined by:

1. Inner slope  $\gamma$
2. Break radius  $r_b$
3. Outer slope  $\beta$
4. Surface brightness  $I_b$

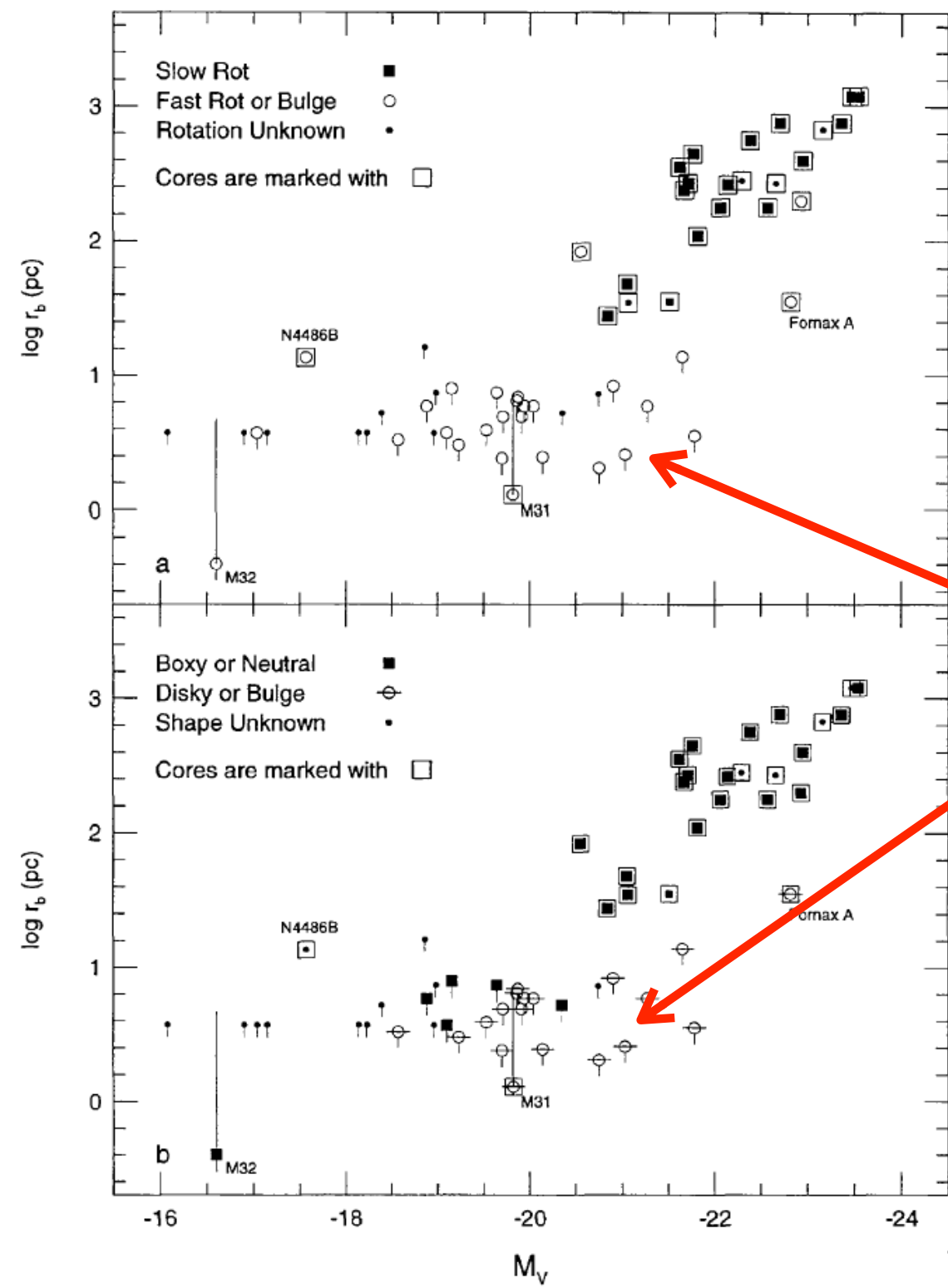
# Bright ellipticals have:

- Cores
- Slow rotation
- Boxy isophotes



# Faint ellipticals have:

- Power-law centers
- Fast rotation
- Disky isophotes



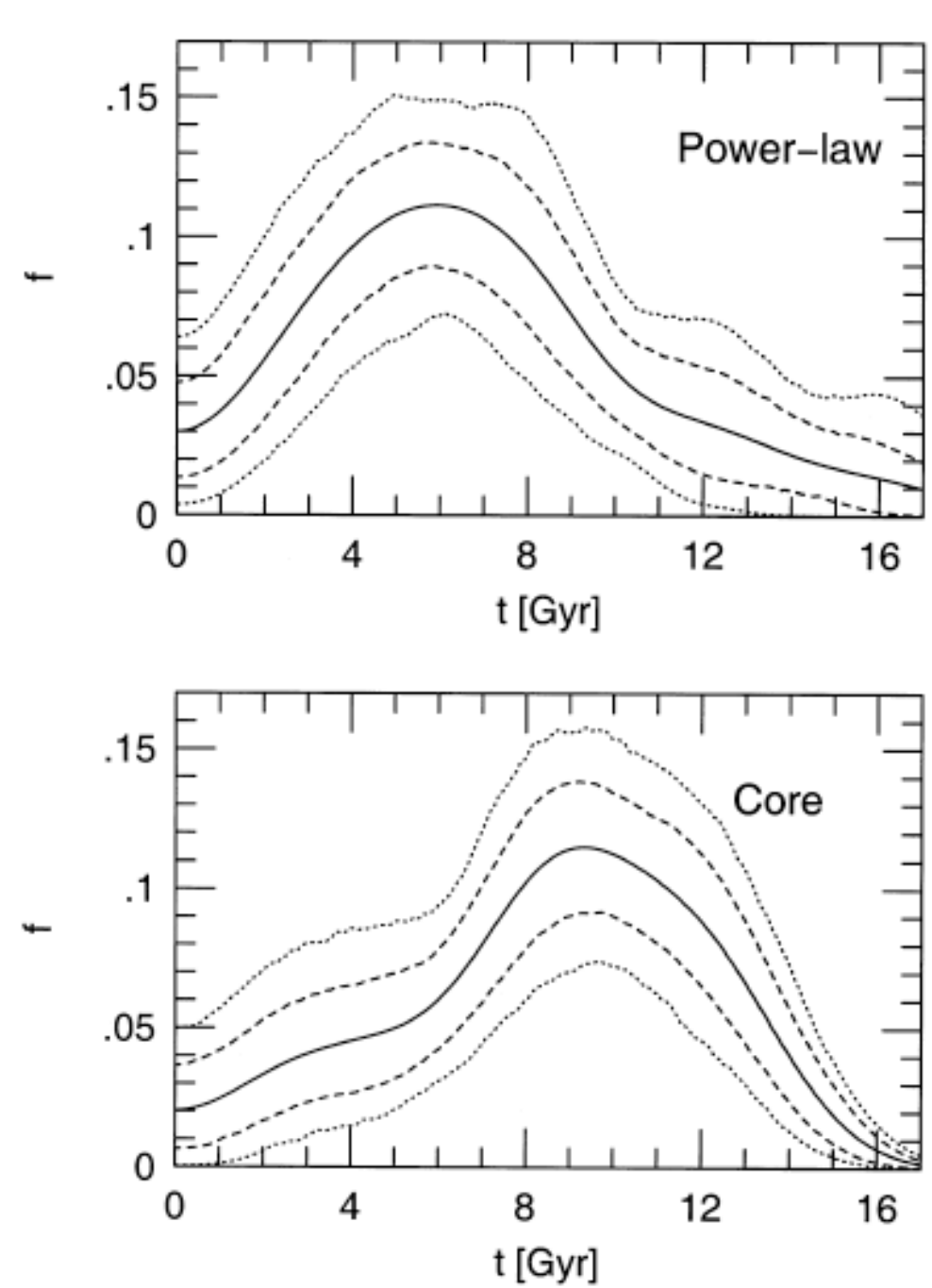


**Figure 3.** (Upper panel) The distribution function for the ages of power-law galaxies, as found by a kernel density estimator. The solid line is the best fit, the dashed lines are the 80 per cent confidence interval, and the dotted lines are the 98 per cent confidence interval. (Bottom panel) The same information for the core galaxies in the sample.

Galaxies with  
power law cores  
also tend to contain  
younger stars.

# 3-Dimensional shapes of ellipticals depends on mass as well...



1. Oblate ( $a = b > c$ )
2. Prolate ( $a > b = c$ )
3. Triaxial ( $a \neq b \neq c$ )

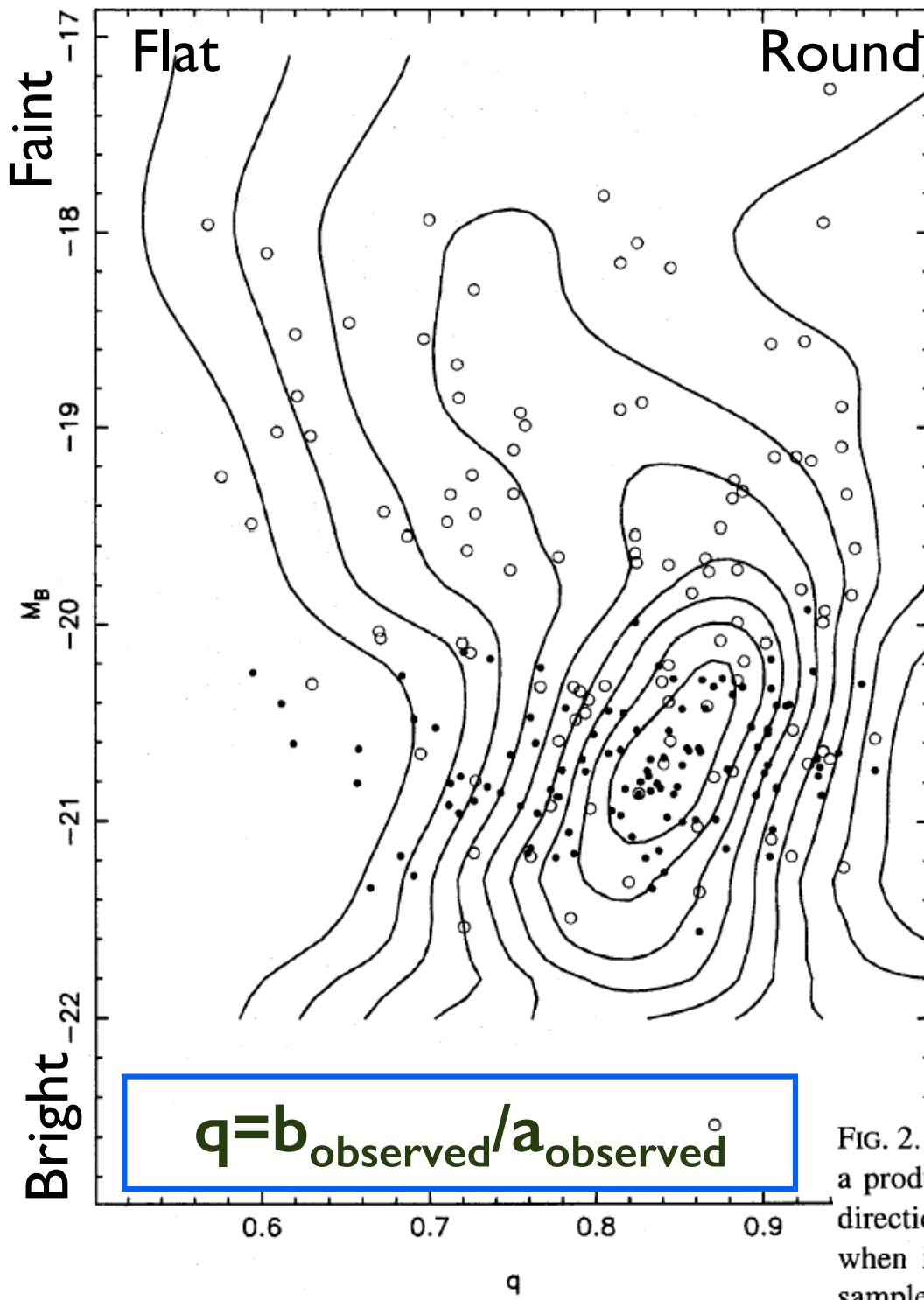


$a, b, c$  are the long, intermediate, and short axis lengths ( $a \geq b \geq c > 0$ )

## Triaxiality parameter

$$\epsilon_1 = 1 - \frac{c}{a}, \quad \epsilon_2 = 1 - \frac{b}{a}$$

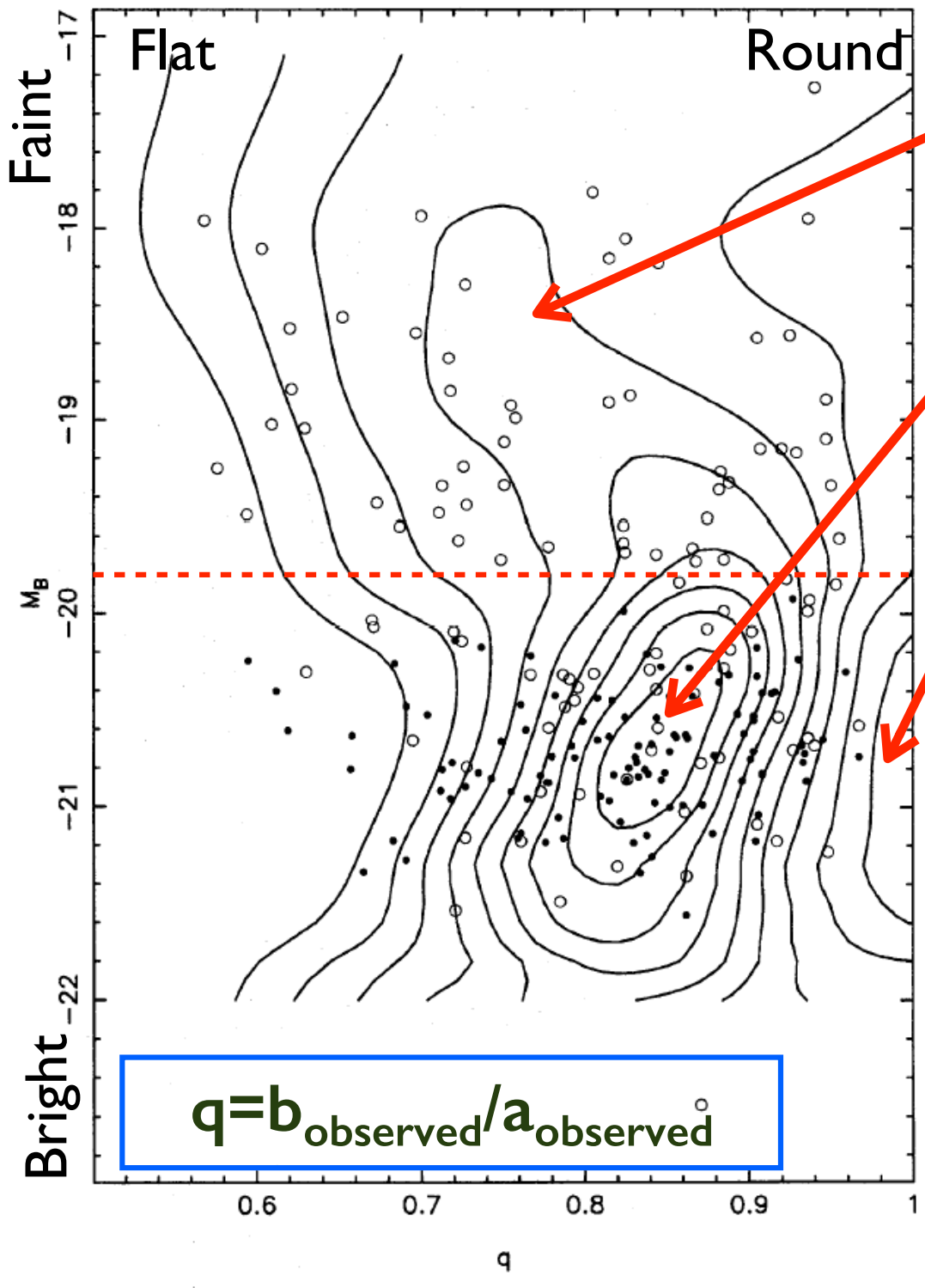
$$T = \frac{a^2 - b^2}{a^2 - c^2} = \frac{\epsilon_2(2 - \epsilon_2)}{\epsilon_1(2 - \epsilon_1)}$$



Assume a triaxiality  $T$ ,  
and do nasty, nasty  
math to invert the  
observed distribution  
of  $q = b/a$ .

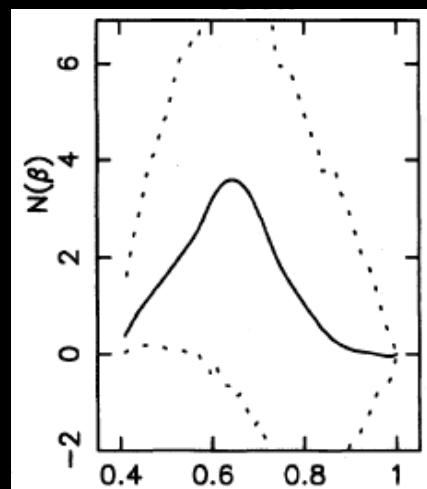
Observed distribution,  
& smoothed estimate  
of the observed  
distribution

FIG. 2. Estimate of  $f(q, M_B)$  for the 220 galaxies in our sample, obtained via a product-kernel technique with different window widths in the  $q$  and  $M_B$  directions. The function  $f$  has been normalized at every  $M_B$  to give unit area when integrated along  $q$ . Circles are galaxies in the Djorgovski—Ryden sample; dots are from the Lauer—Postman sample. The six galaxies in both samples are indicated by circles. Contours are separated by 0.5 in  $f$ .

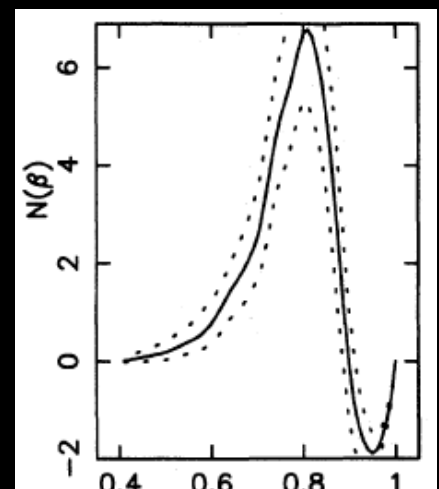


1. Faint ellipticals are flatter.
2. Bright ( $M_B < -20$ ) are rounder.
3. But, no truly round ellipticals are seen.

Recovered  $q$  distributions:



$M_B \approx -18.5$



$M_B \approx -20.5$

(x-axis =  $b/c$ , assuming oblate)

# Bright ellipticals:

- 1. Cores
- 2. Slow rotation
- 3. Boxy isophotes
- 4. Older stellar ages
- 5. Low peak phase space density

Gas Poor Mergers

# Faint ellipticals:

- 1. Power-law centers
- 2. Fast rotation
- 3. Disky isophotes
- 4. Younger stellar ages
- 5. High peak phase space density

Gas Rich Mergers

# Bright ellipticals:

- 1. Cores
- 2. Slow rotation
- 3. Boxy isophotes
- 4. Older stellar ages
- 5. Low peak phase space density

# Faint ellipticals:

- 1. Power-law centers
- 2. Fast rotation
- 3. Disky isophotes
- 4. Younger stellar ages
- 5. High peak phase space density

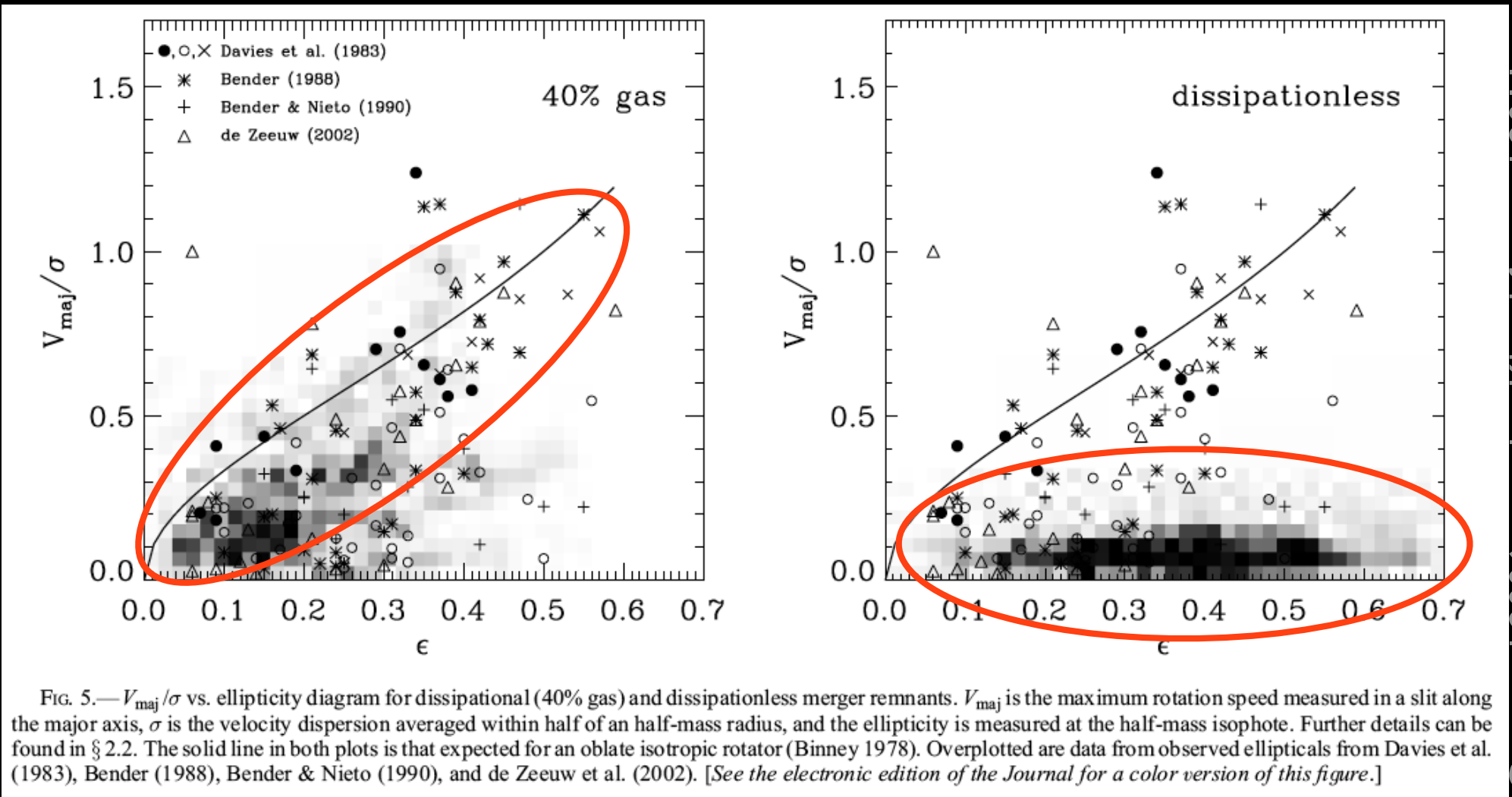
## Gas Poor Mergers

- 1. No star formation
- 2. No increase in central density to boost phase space density
- 3. No preferred axis, so rounder

## Gas Rich Mergers

- 1. Gas settles to center.
- 2. Gas becomes diskier
- 3. New stars form, making cusp
- 4. Isophotes become disk-like
- 5. Phase space density ↑
- 6. Younger stars due to #3

# Simulations of gas rich vs star-only mergers



Gas poor = velocity anisotropy dominates

Bright  
ellipticals:

Gas Poor Mergers

Faint  
ellipticals:

Gas Rich Mergers

Is the difference due to:

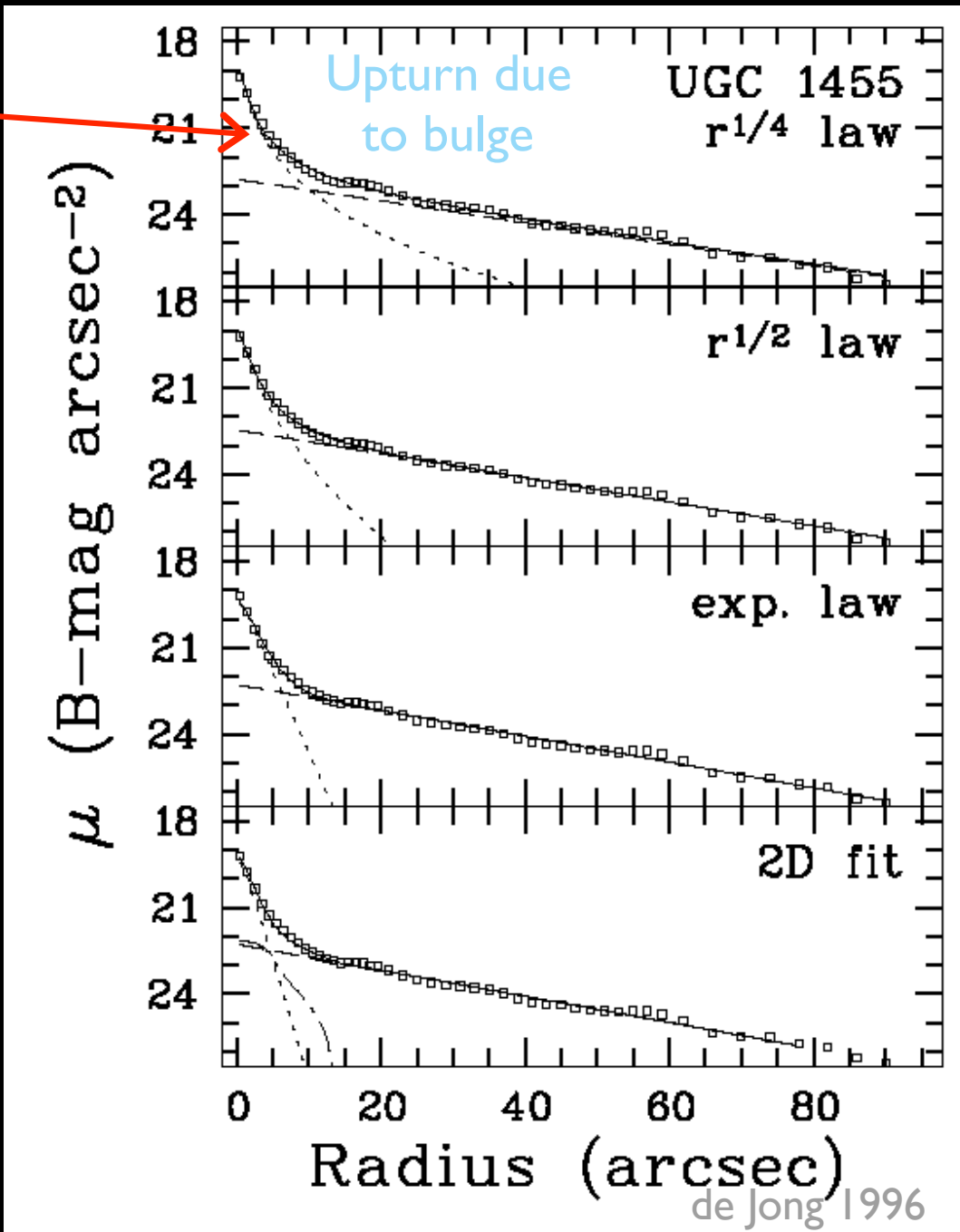
- Timing (is gas used up before epoch of last major merger?)
- Feedback (are winds driven by central black holes more effective at keeping gas out?)

# Structure of Bulges

- Tricky!
- Profile depends on mass.
- More massive bulges are more deVaucouleurs.
- Late-type galaxy bulges may be “pseudobulges”, built from disk material

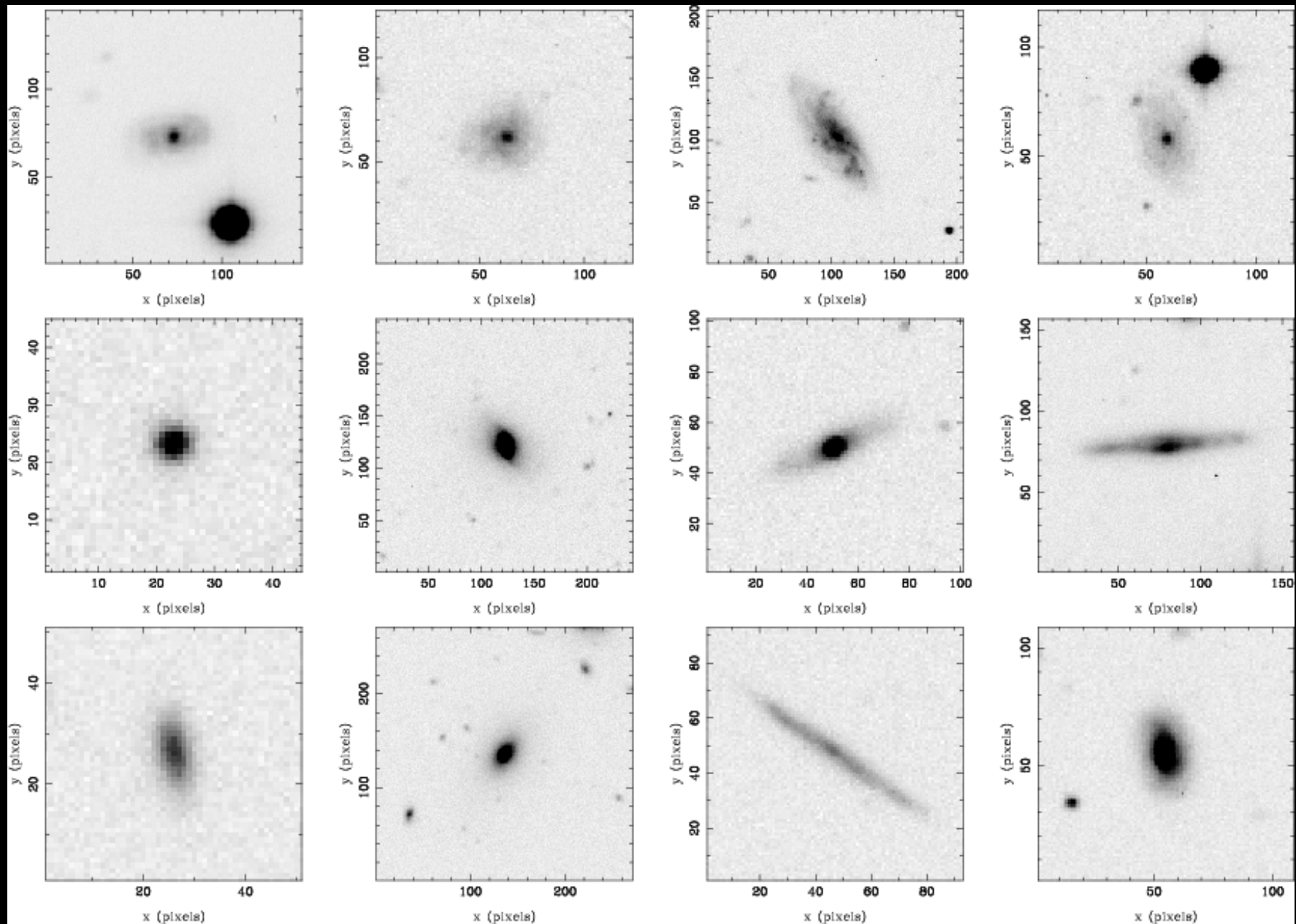
# Surface Photometry of Bulges

- Hard to separate the bulge from the disk.
- Can fit 1-d profiles or 2-d profiles.
- Latter is more robust.

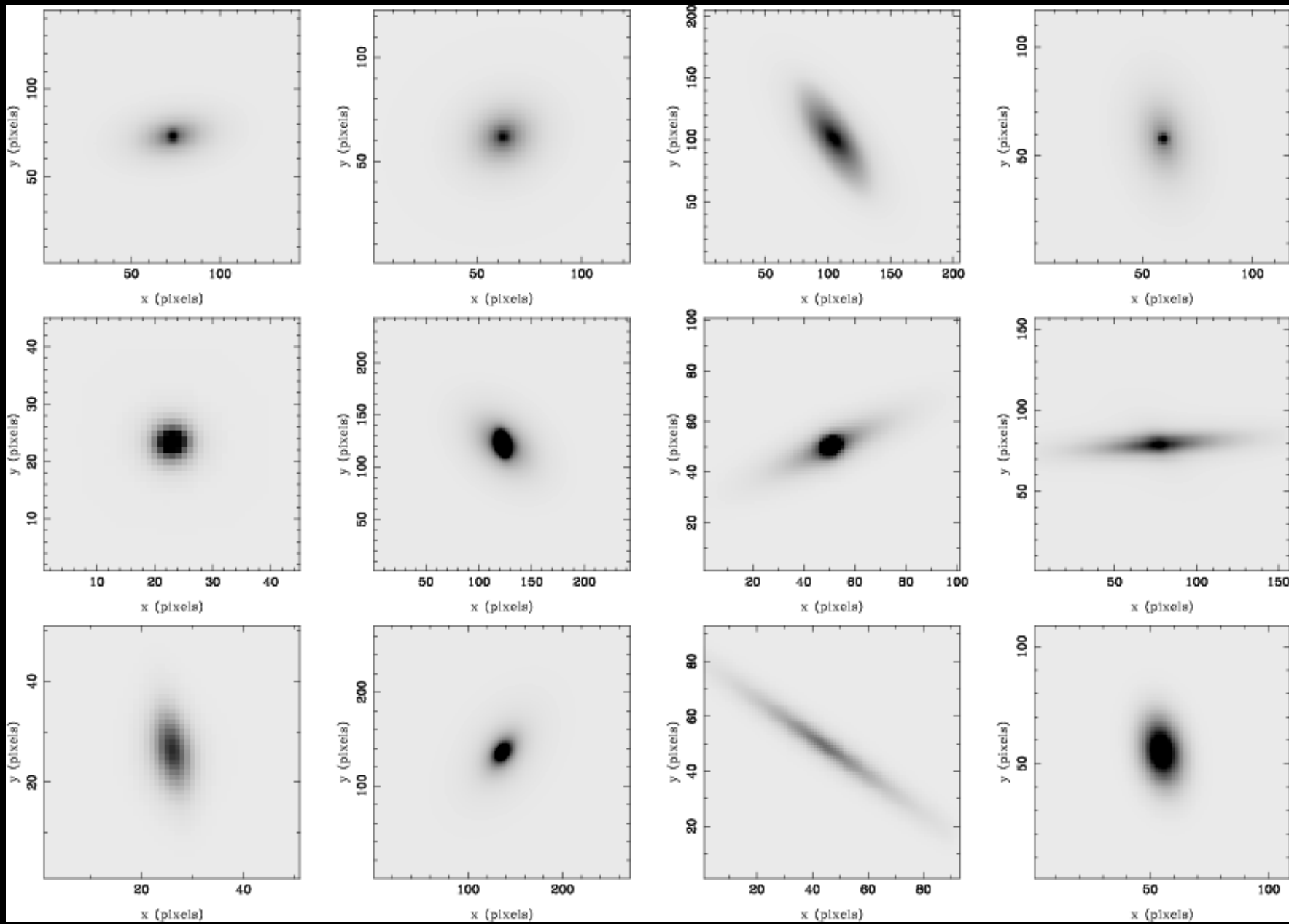


Acceptable fits for many different choices of bulge profiles

# Data



# Model



# Bulge sizes vs Disk sizes

Typically,  
 $r_e \sim h/5$

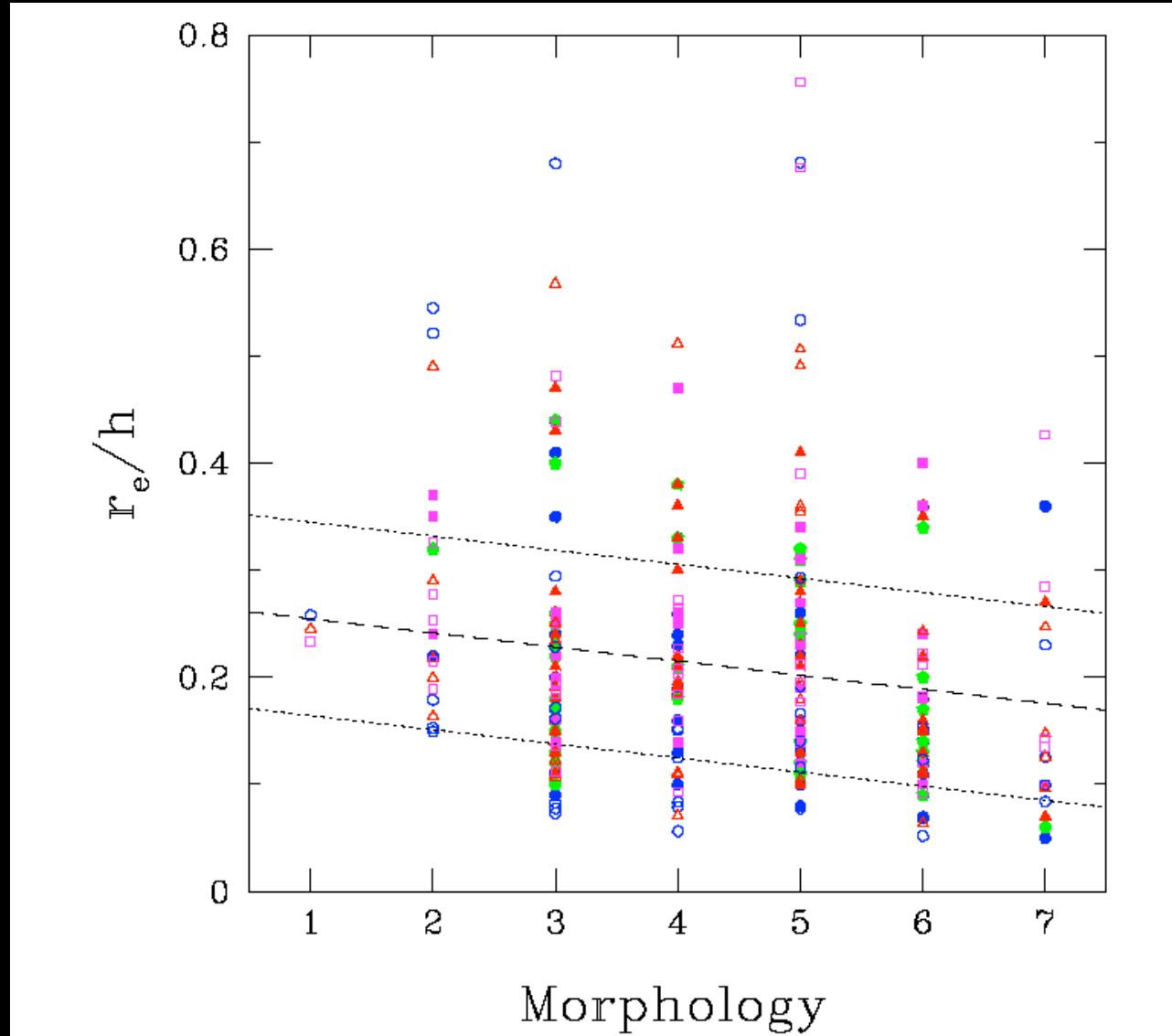
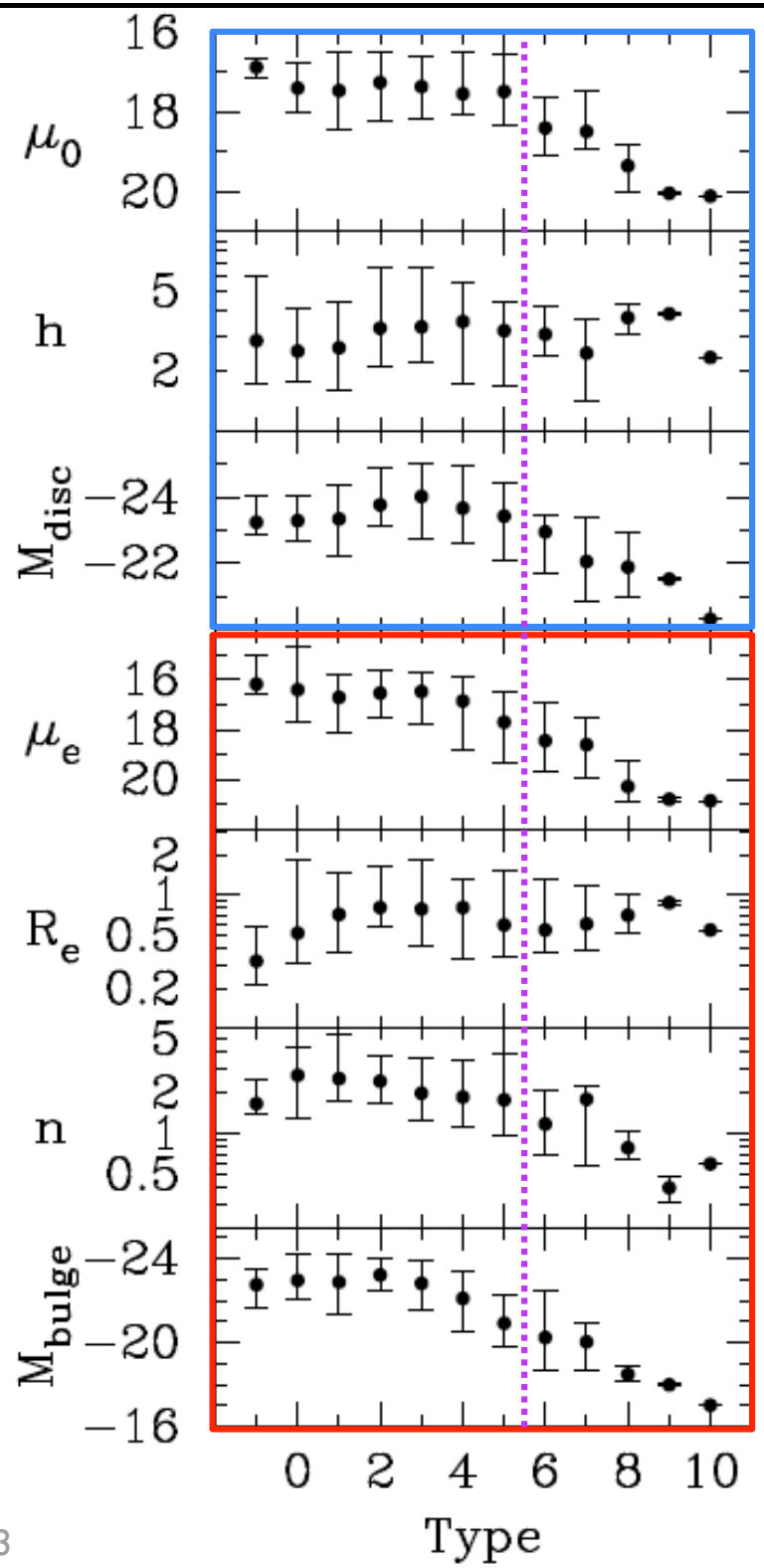


Fig. 21.— Distribution of  $r_e/h$  with Hubble types for our Type-I galaxies and those of Graham (2001). Symbols and colors are as in Fig. 20. The dashed line describes the fit  $\langle r_e/h \rangle = 0.20 - 0.013(T - 5)$  with  $1\sigma = 0.09$  errors (dotted lines) based on our data only.

# Surface Brightness vs Mass trend imprints morphologically: $\mu$ tends to fall for late-type galaxies ( $T>Sc$ )



A manifestation of the fact that later types are fainter, and fainter galaxies have lower surface brightness. Note also that Sa-Sc's are similar.

Graham & Worley 2008

**Figure 3.** Standard  $(K\text{-band})$  disc and bulge structural properties as a function of galaxy Type. For the disc,  $\mu_0$ ,  $h$  and  $M_{\text{disc}}$  are the central surface brightness, scale-length and absolute magnitude. For the bulge,  $\mu_e$ ,  $R_e$ ,  $n$  and  $M_{\text{bulge}}$  are the effective surface brightness, effective half-light radius, Sérsic index and absolute magnitude. The data have been taken from Table 3, except for the bulge magnitudes which have been taken from Table 4. For each T-Type, the median is marked with a circle and the ‘error bars’ denote the 16 and 84 per cent quartiles of the full distribution, rather than uncertainties on the median value.

### 3. Disk Scale Length vs Surface Brightness

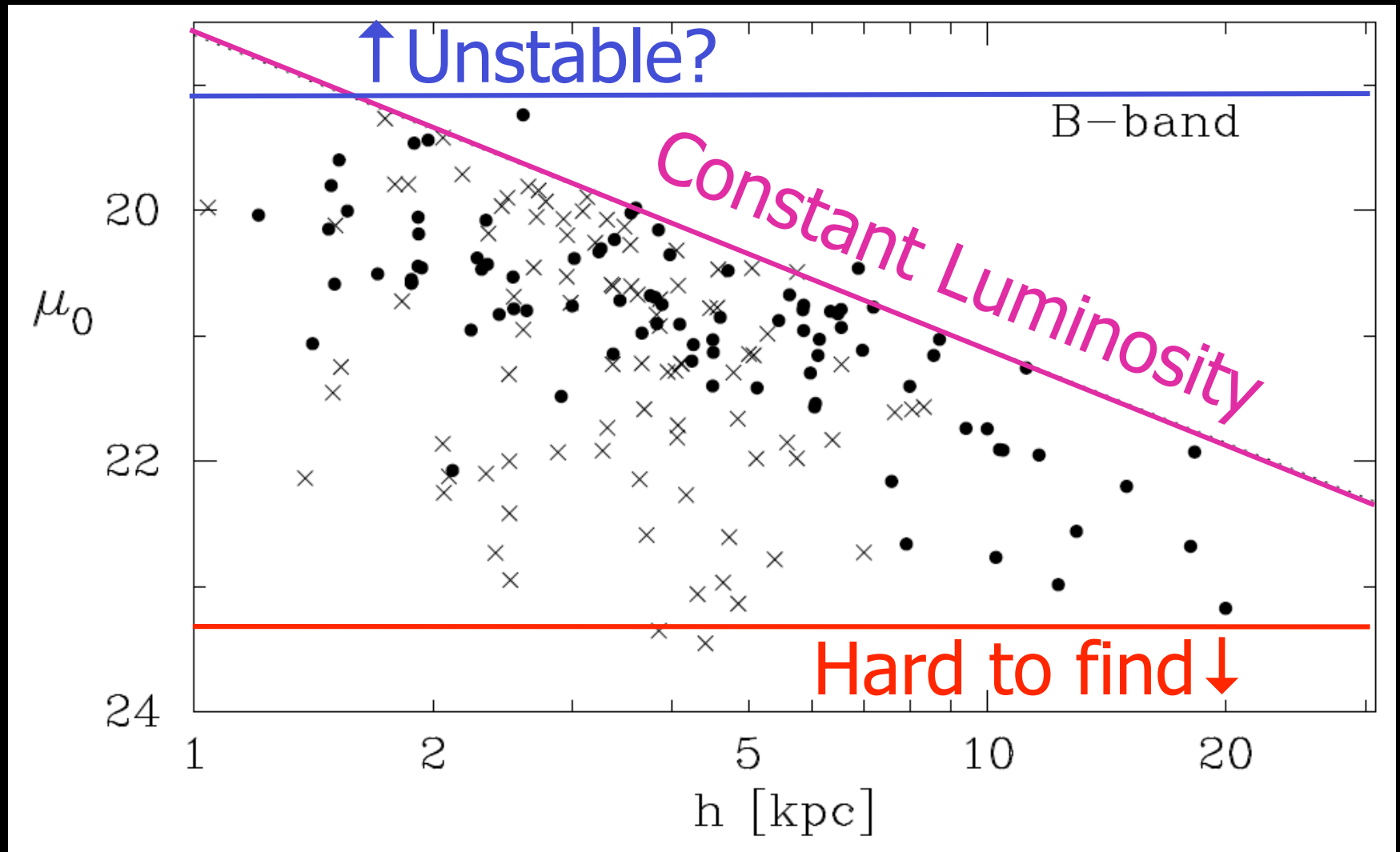
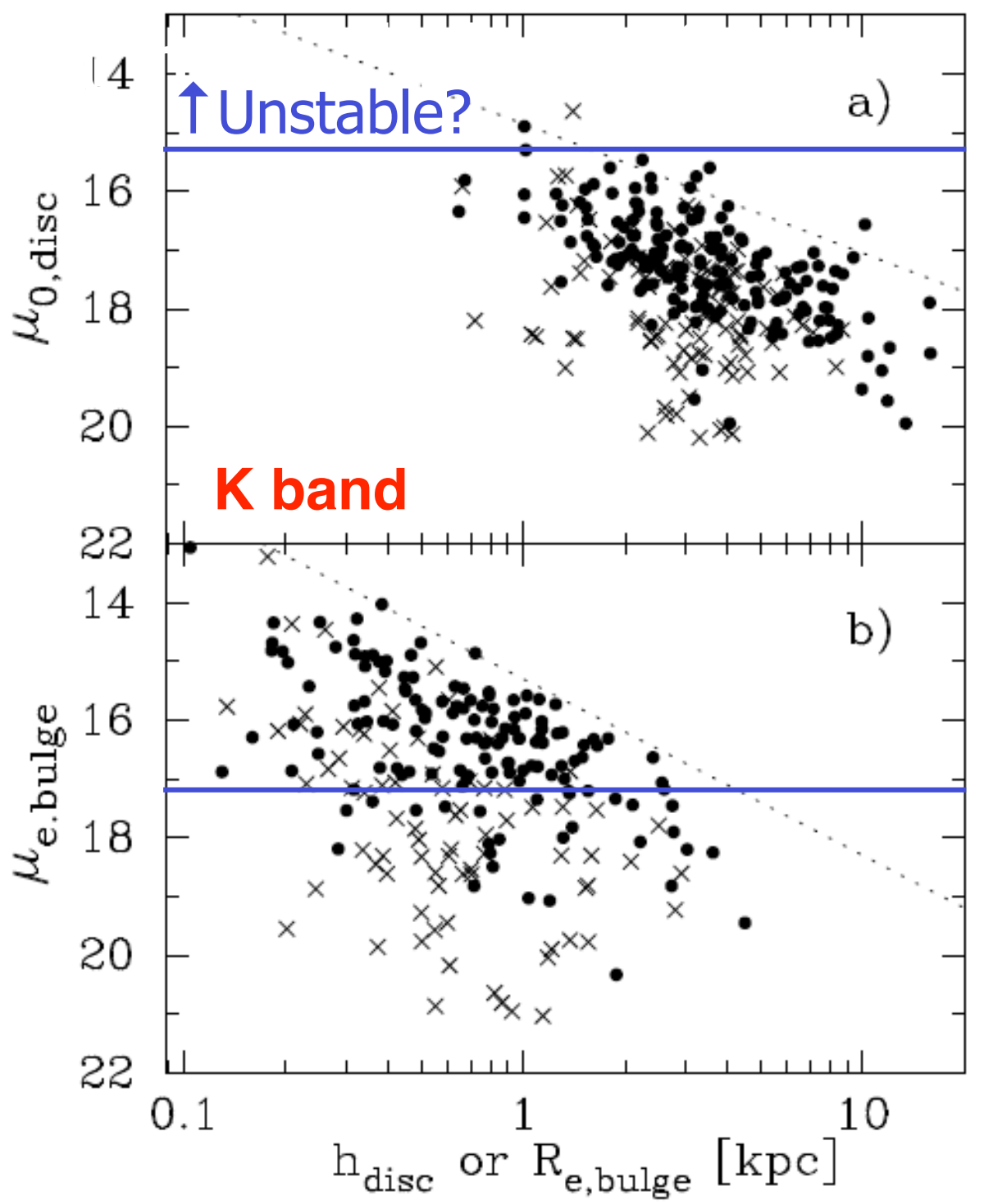


**Figure 9.** *B*-band. Central disc surface brightness (corrected using equation 1) versus disc scalelength (corrected using equation 2). Rather than a Freeman (1970) law of constant surface brightness, an upper bright envelope, which has been seen before (e.g. Graham 2001b and references therein), is evident. The empirically-fitted dotted line in this diagram is such that  $\mu_{0,bright} = 18.6 + 2.5 \log h$ . Galaxy types Sbc ( $T = 4$ ) and earlier are denoted by circles, while later galaxy types are denoted by crosses. The noticeably broader distribution for the late-type disc galaxies has also been noted before (Graham & de Blok 2001).

# For example

Horizontal line is at  
same  $\alpha_e$  for  $n=1$

**Figure 8.** *K*-band. Top panel: Central disc surface brightness (corrected using equation 1) versus disc scalelength  $h$  (corrected using equation 2). Bottom panel: Bulge effective surface brightness (observed) versus the bulge effective radius  $R_e$  (observed). The upper bright envelope is traced here with the (empirical) lines  $\mu_{0,bright} = 14.85 + 2.2 \log h$  (panel a) and  $\mu_{e,bright} = 15.3 + 3.0 \log R_e$  (panel b). Galaxy types Sbc ( $T = 4$ ) and earlier are denoted by the circles, while later galaxy types are denoted by the crosses.



# Bulge Pr

$$\Sigma(r) = \Sigma_e e^{-\kappa[(r/r_e)^{1/n} - 1]}$$

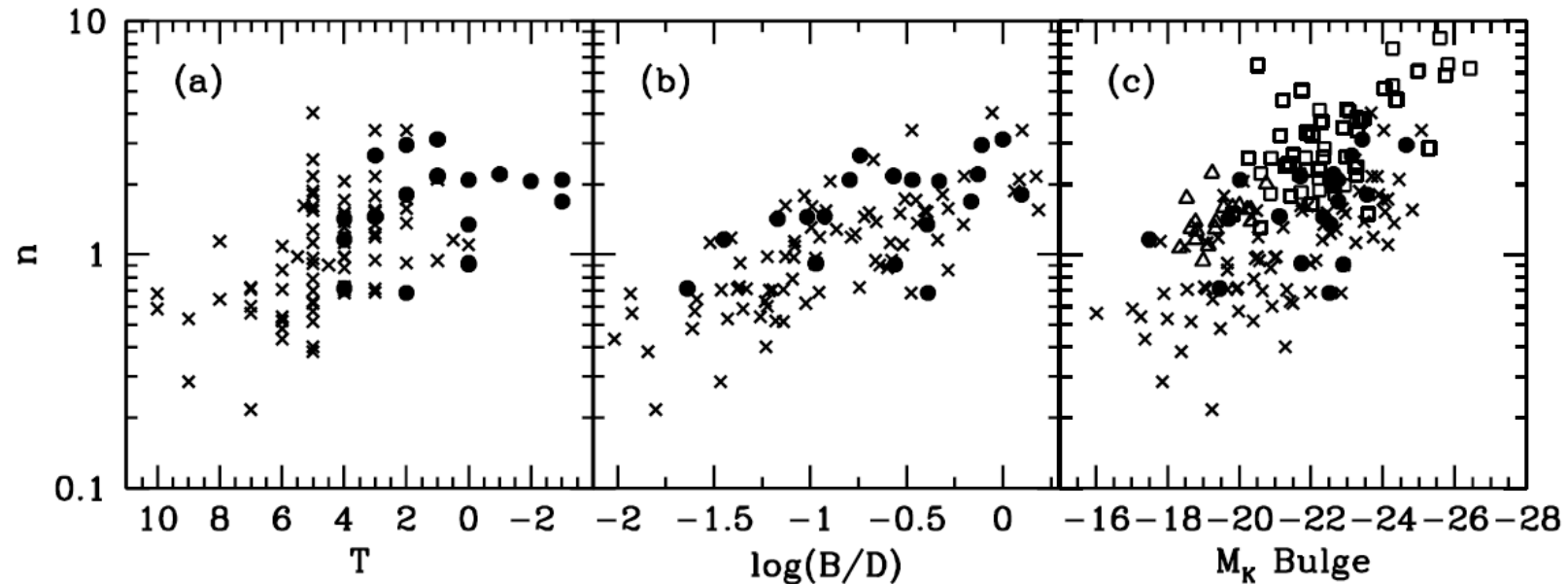
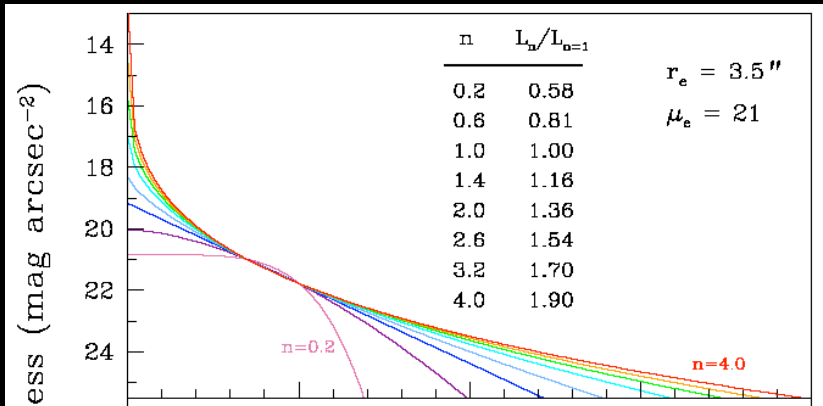


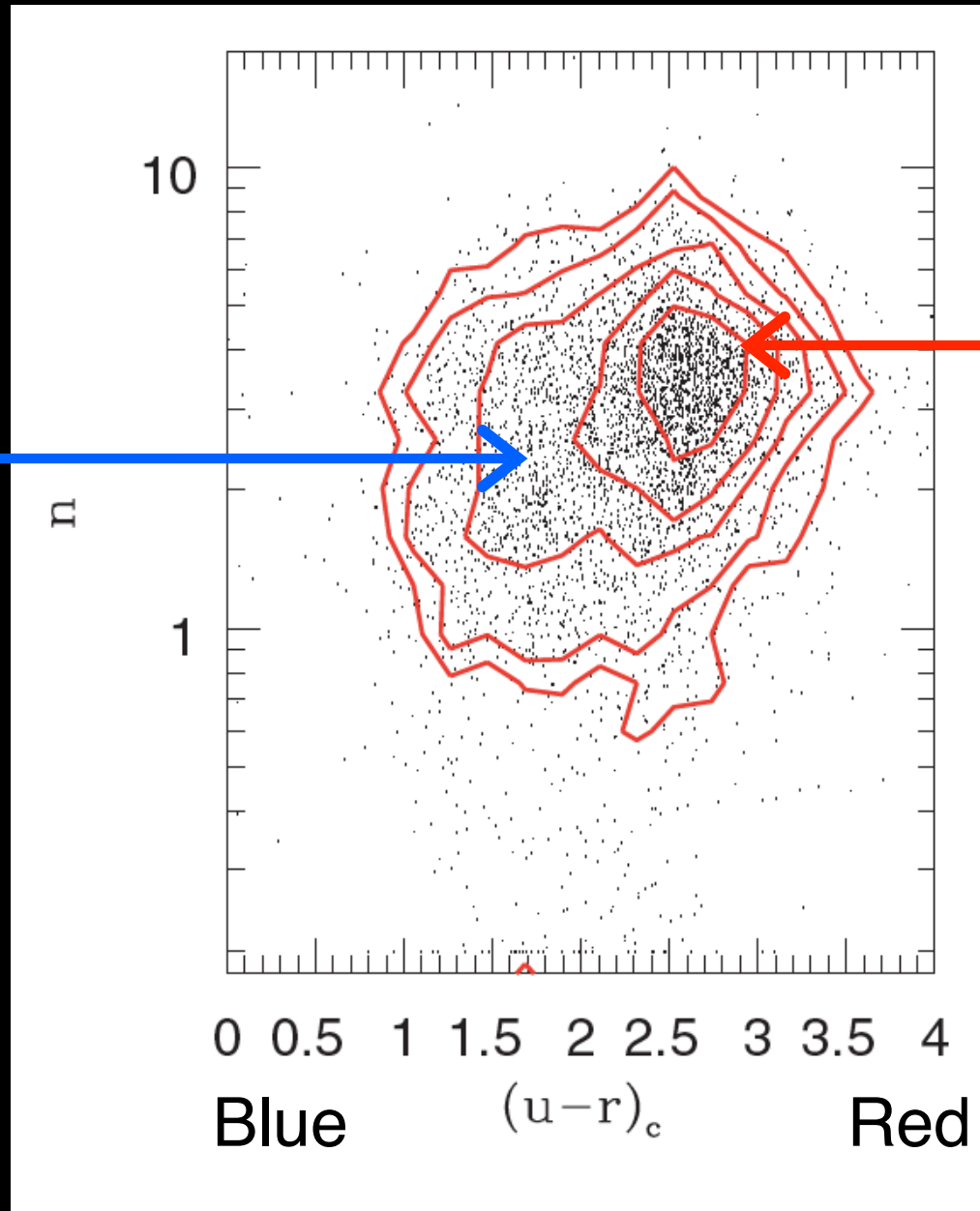
FIG. 6.— The bulge Sérsic index  $n$  is plotted against: (a) the revised morphological type index  $T$  from the RC3; (b)  $B/D$  derived from the best-fit parameters; and (c) the bulge  $K$ -band absolute magnitude derived from  $B/D$  and the galaxy  $K$ -band absolute magnitude, corrected for Galactic extinction, cosmological dimming and  $K$ -correction. *Filled circles*: bulges, this work. *Crosses*: bulges from the de Jong & van der Kruit (1994) sample, as analyzed by Graham (2001a, 2003). *Triangles*: Coma dwarf ellipticals from Graham & Guzmán (2003). *Squares*: Virgo ellipticals from Caon et al. (1993).



Late-type galaxy bulges are more exponential ( $n=1$ ) than deVaucouleurs ( $n=4$ )

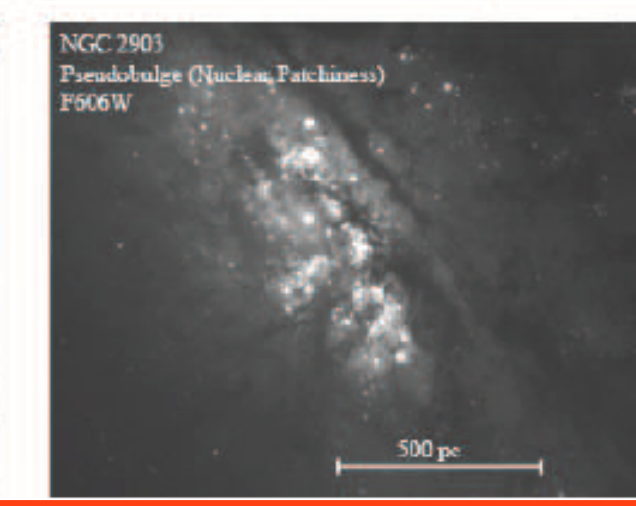
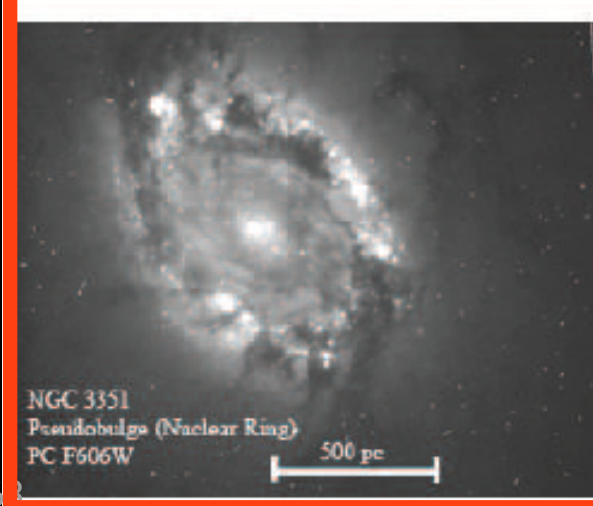
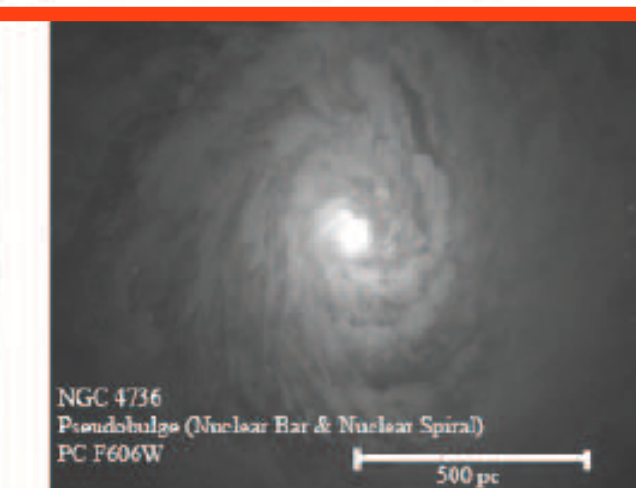
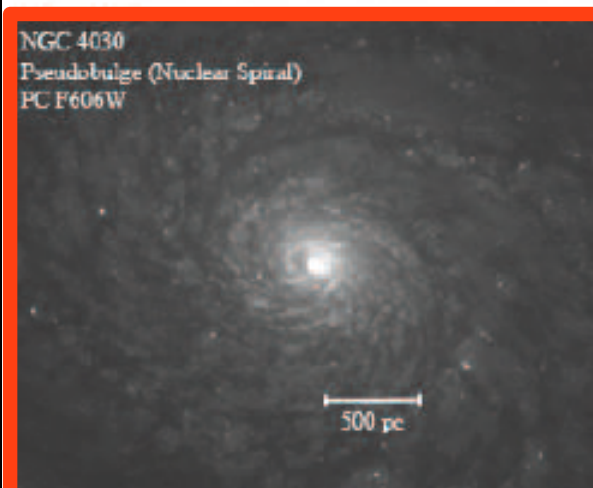
# Two Types of Bulges?

“Psuedo-Bulge”



“Classical”

# Classical Bulges

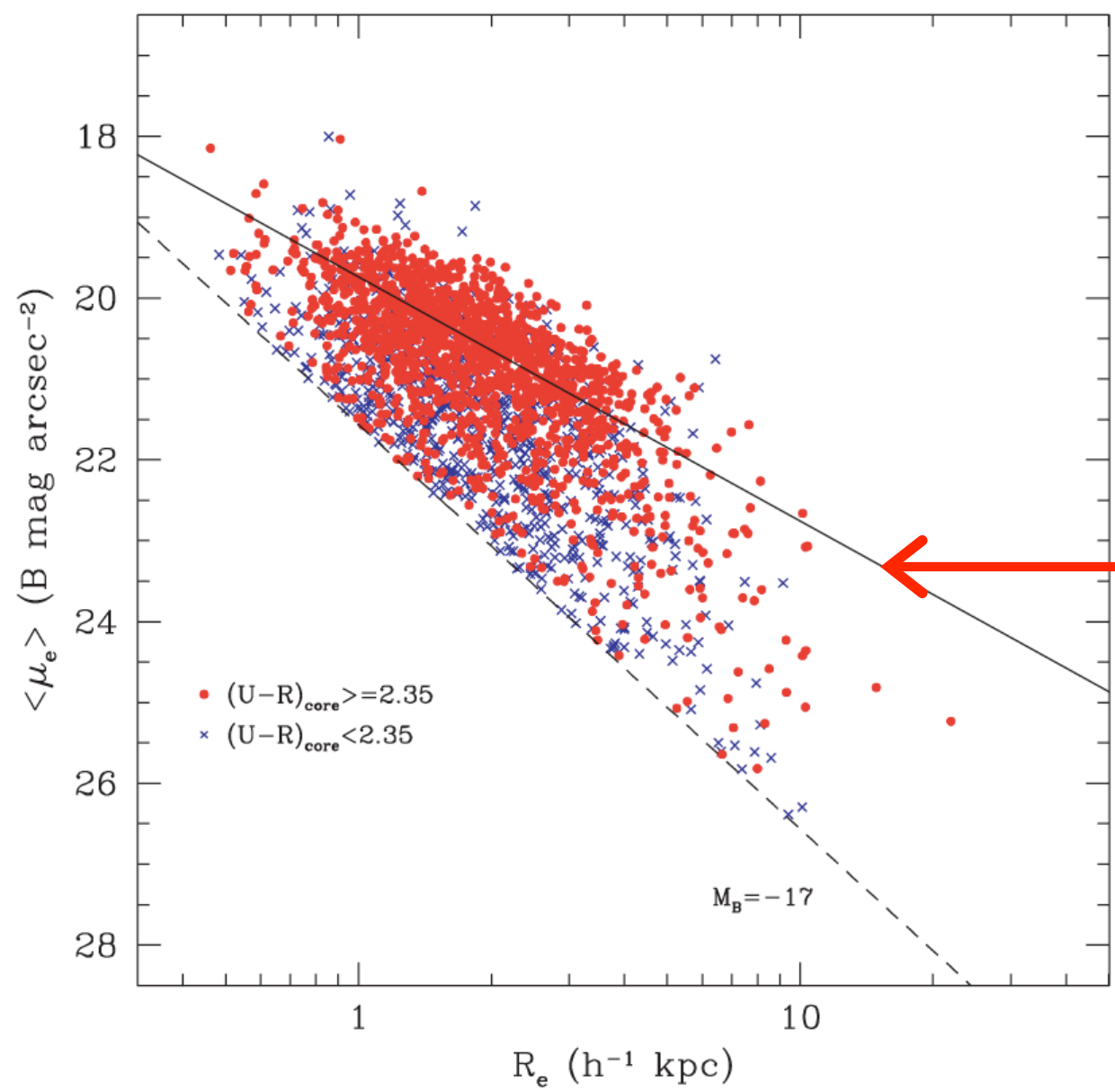


“Pseudo-  
bulges”

HST Observations

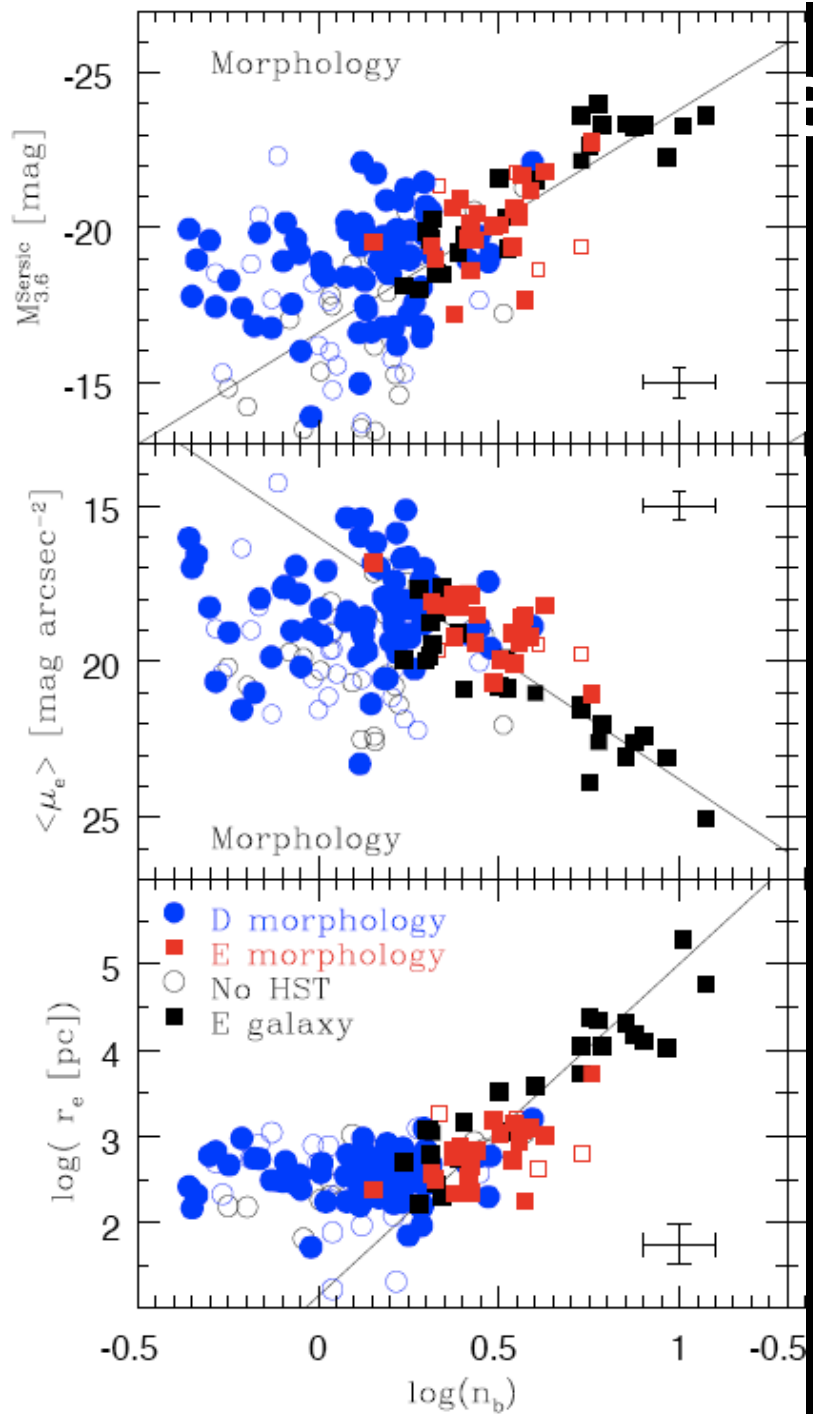
Fisher & Drory 2010

# Structurally, classical bulges are similar



“Kormendy Relation”  
for ellipticals (1977)

# “bulges” have $n < 2$ and weak



Based on decompositions of HST images

We define “bulges” photometrically, as excess light over the inward extrapolation of the surface brightness profile of the outer disk. The region of the galaxy where this excess light dominates the profile is the bulge region. We classify galaxies as having a pseudobulge by their morphology within this bulge region; if the bulge is or contains any of the following features: a nuclear bar, a nuclear spiral, and/or a nuclear ring, then the bulge is called a pseudobulge. Conversely, if the bulge better resembles an elliptical galaxy (relatively featureless isophotes), then the bulge is called a classical bulge. This method is discussed in KK04. The existence/absence of visibly identifiable disk-like structure in a bulge correlates with properties of the bulge and the whole galaxy. The same method is shown to be successful in identifying bulges with higher specific star formation rates (Fisher 2006) and globally bluer galaxies (Drory & Fisher 2007).

Fisher & Drory 2010

FIG. 7.— Correlations of the bulge Sérsic index with (from bottom to top) half-light radius of the bulge (a), average surface brightness within the half-light radius (b), and magnitude of the bulge at  $3.6 \mu\text{m}$  (c). In all panels, pseudobulges are represented by blue circles, classical bulges by red squares, and elliptical galaxies by black squares. Galaxies in the high quality sub-sample are shown as filled symbols whereas galaxies that do not meet criteria for the high-quality data set (see text) are shown as open symbols.

# Bulge Form

- Primordial  
Elliptical that accretes a disk? ("classical bulge")
- "Secular"  
Bulge grows through disk instabilities  
("pseudobulge")

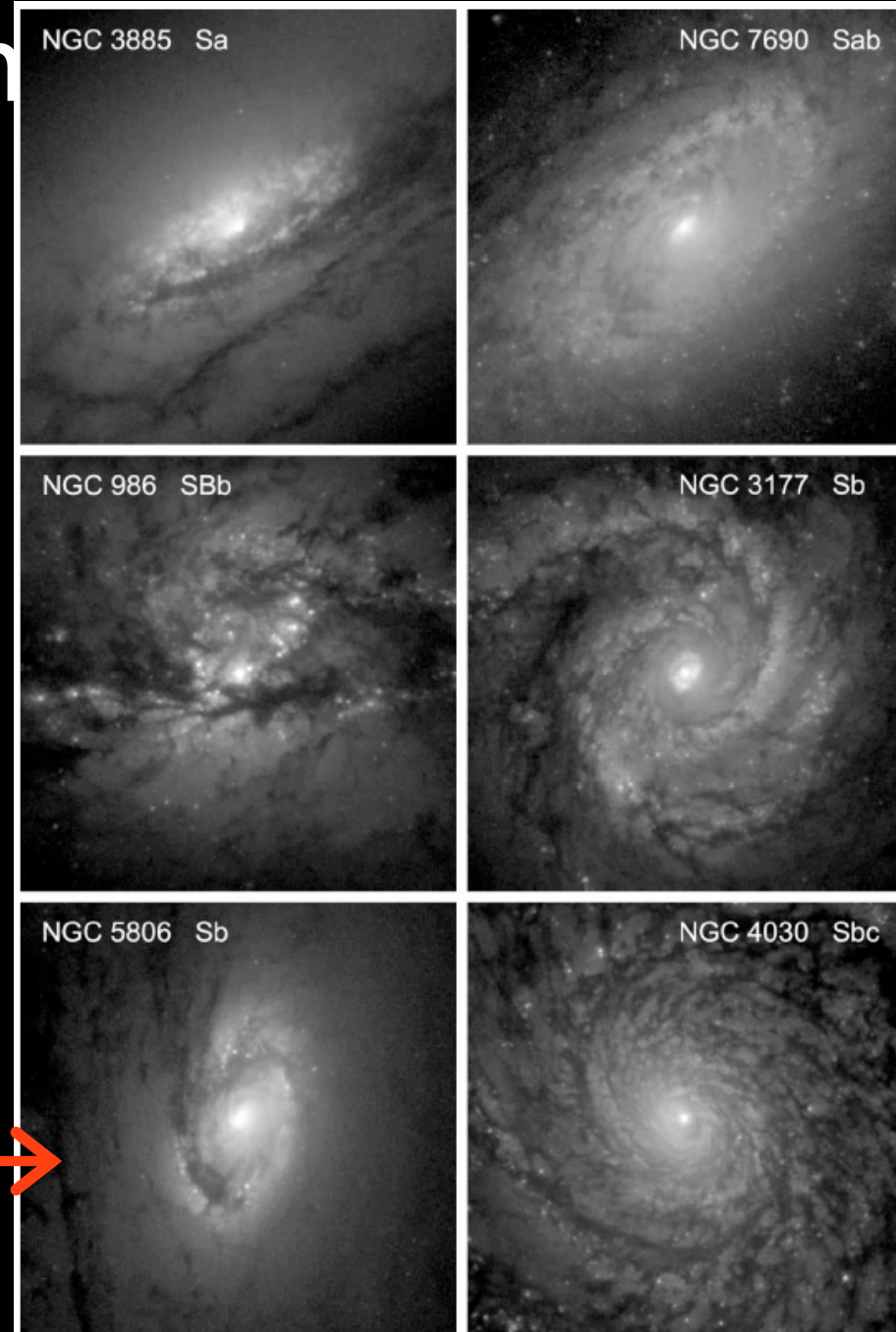
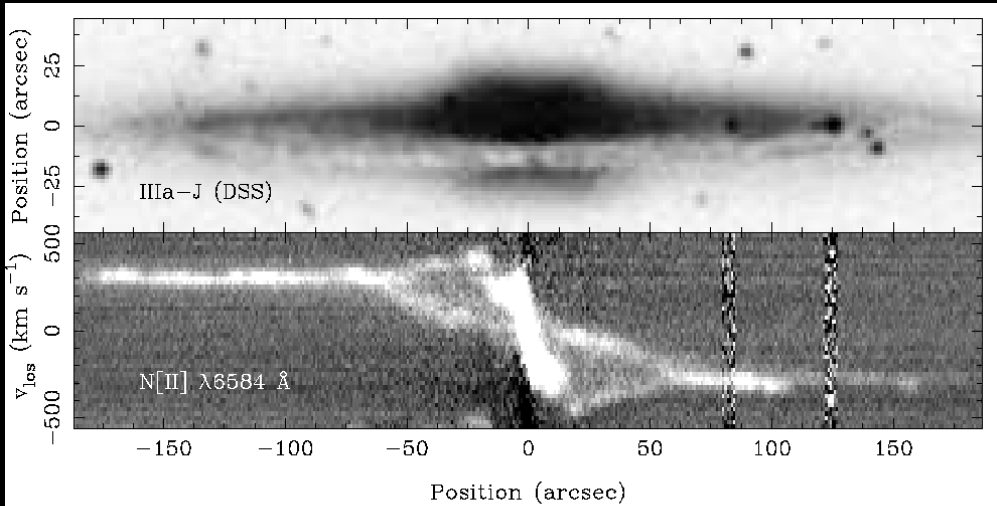
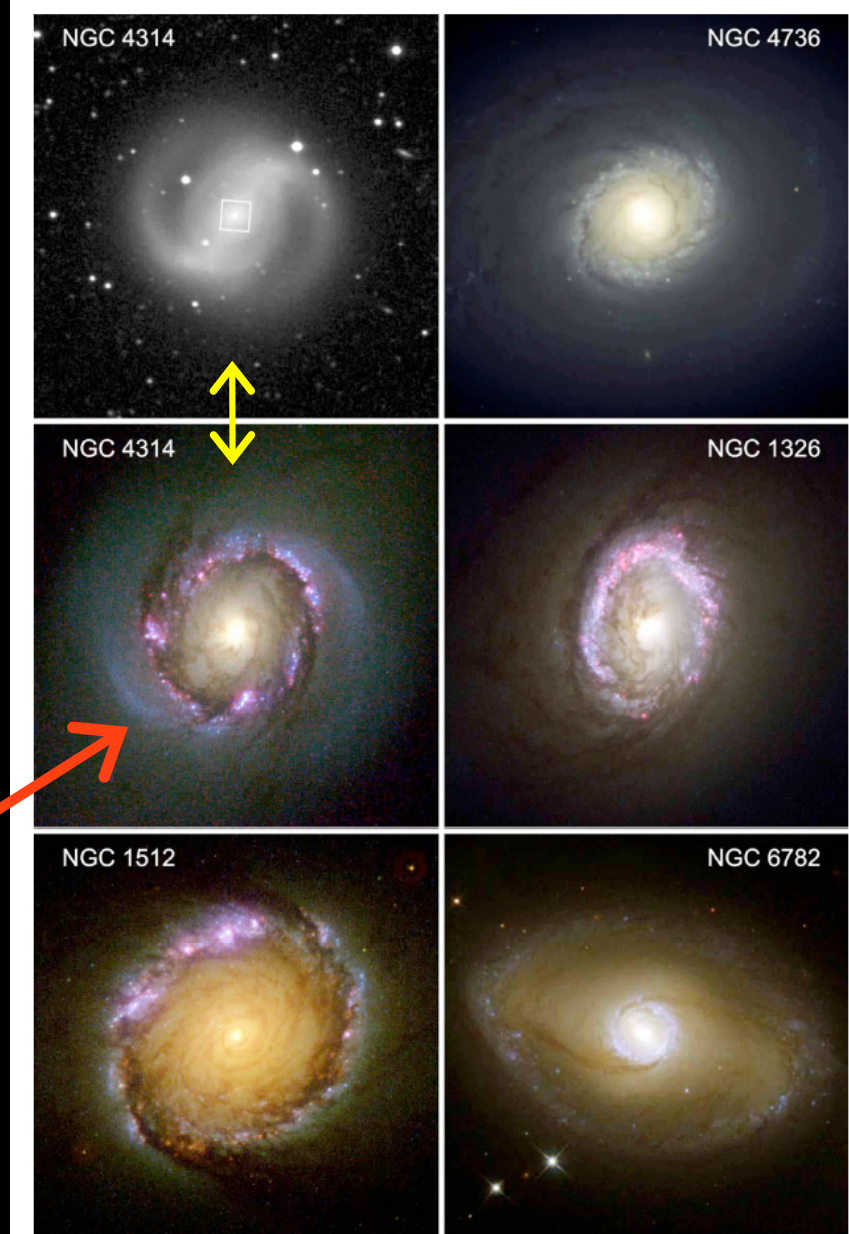


Figure 5. Sa – Sbc galaxies whose "bulges" have disk-like morphology. Each panel shows an  $18'' \times 18''$  region centered on the galaxy nucleus and extracted from HST WFPC2 F606W images taken and kindly provided by Carollo et al. (1998). North is up and east is at left. Displayed intensity is proportional to the logarithm of the galaxy surface brightness.



*Figure 15* (Top) NGC 5746 (Sb) has a prominently box-shaped bulge (see also Sandage & Bedke 1994). (Bottom) Position-velocity diagram of the [N II]  $\lambda 6584 \text{ \AA}$  emission line along the major axis registered in position with the image. The “figure 8” pattern is interpreted as the signature of a barred galaxy by Bureau & Freeman 1999, who kindly supplied this figure) and by Kuijken & Merrifield (1995).

Bar builds up vertical structure. Nuclear star formation then builds high surface brightness.



*Figure 8* Nuclear star formation rings in barred and oval galaxies. For NGC 4314, a wide-field view is at top-left; for NGC 4736, the wide-field view is in Figure 2. Sources: NGC 4314 – Benedict et al. (2002); NGC 4736 – NOAO; NGC 1326 – Buta et al. (2000) and Zolt Levay (STScI); NGC 1512 – Maoz et al. (2001); NGC 6782 – Windhorst et al. (2002) and the Hubble Heritage Program.